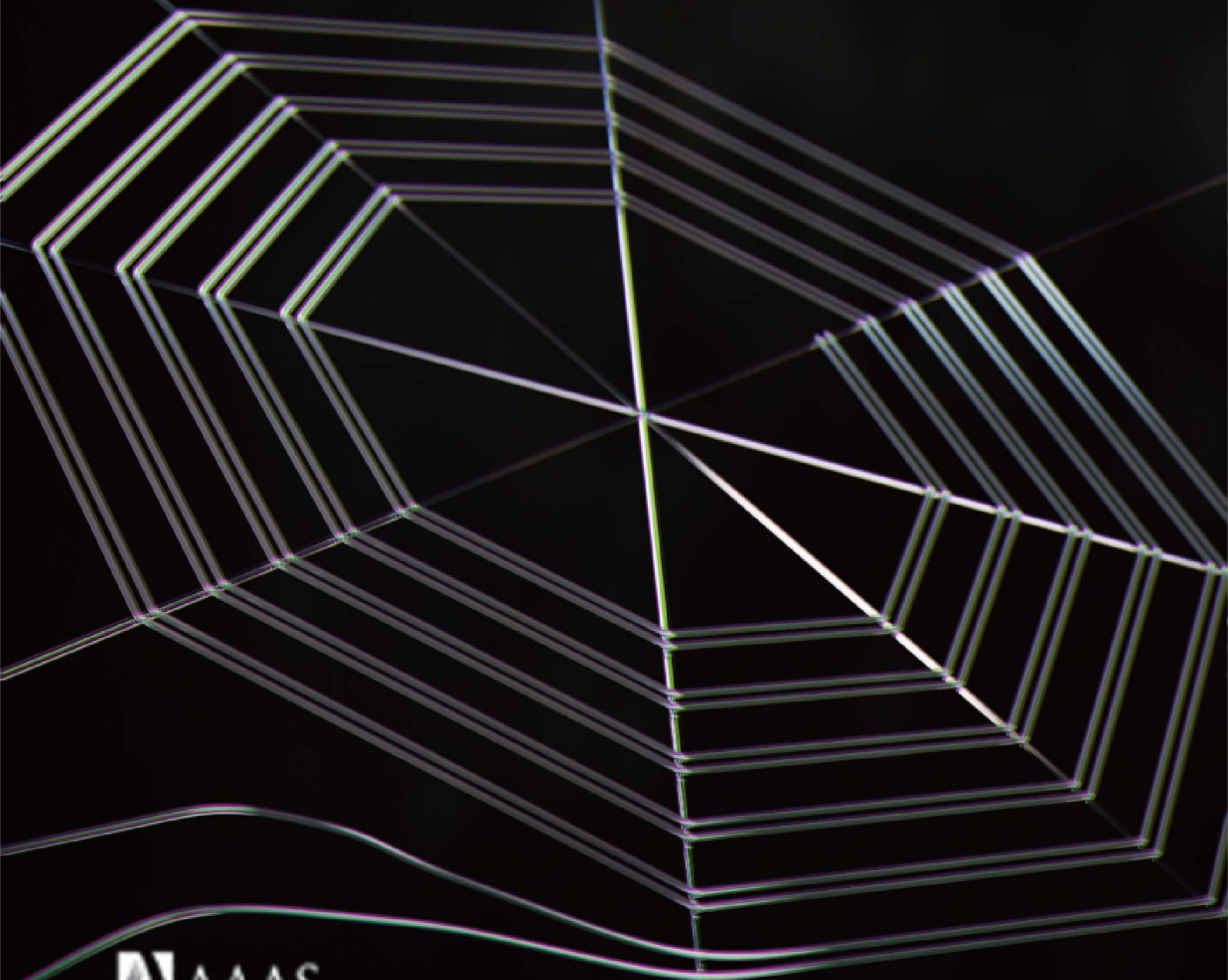# Science
Robotics

BIOMIMETICS

Spinning artificial spider webs

Jonathan Rossiter

Sensing, adhesion, and self-cleaning capabilities are demonstrated in artificial spider webs through electrostatic actuation and a dirt-shirking coating.

Arachnids have long been the focus of study for materials development and robotics: Spiders employ a unique hybrid locomotion system, using hydraulic pressure generated in the prosoma organ to power their powerful yet thin legs (1); their webs have amazing self-tensioning behaviors, exploiting the surface tension of water droplets (2); and spider dragline silk has a specific tensile strength five times that of steel at around 1.3 GPa. In addition to these amazing characteristics, spiders, as carnivores, use high-fidelity sensing and filtering coupled to their web structures to sense and locate prey and to determine when to attack. Scientists have been fascinated by arachnid biology and have sought to mimic spider actuation and sensing and the sophisticated structures and materials of spider silk and spider webs. Writing in *Science Robotics*,

Lee and colleagues (3) have brought together the fields of biomimetics, electrostatics, and smart materials to develop a new ionic spider web (ISW) material and to replicate essential behaviors of spiders' webs in self-sensing, self-cleaning, and prey-capturing artificial ISWs (Fig. 1). This adds new capability to robotic systems, with wide potential applications from climbing robots to self-cleaning coatings.

Traditionally, researchers have targeted the strength of spiders' webs through mimicry of the silk extrusion gland (4). This is extremely challenging because the spider has evolved a highly optimum chemical extrusion process involving multiple stages of pH changes, ion infusion, and mechanical fiber alignment. Lee and colleagues (3) have taken a different approach and have developed artificial spider webs that, although not as strong as artificial silks, exhibit novel functionality that is inspired by the materials and structures of spider webs. They have noted that smart materials have limitations in their abilities to actuate, sense, and grip objects and that controlled electrostatics offers a technology to overcome these limitations. Operating at the intersection of these fields, they present a composite coaxial fiber made of ionically conductive and stretchable organogel, encapsulated with silicone rubber to form a strand, which is then perfluorinated using a conformal coating to reduce surface energy. They

used this composite fiber to form a range of ISW structures that resemble the classic planar spider web. By applying and sensing the electrical potential between pairs of ISW fibers, they generated three behaviors. First, electroadhesion can be induced between the web and an object by establishing an electric field between adjacent strands of the web. Second, objects making contact with the web generate an electrical response in the ionic conductors, which can then be used to initiate the adhesion process. Last, by applying a time-varying electric field between pairs of ionic strands, they can be made to vibrate and, thereby, with the help of the hydrophobic coating, throw off contamination. By demonstrating these three characteristics of ISWs, the authors have potentially developed artificial spider web–like structures that can operate in natural, and often dirty, environments.

The value of the work presented by Lee and colleagues extends beyond their immediate use as artificial spider webs. Flexible and stretchable ionic conductors could act as substitutes for conventional conductors, including wires and liquid metal channels, for future electroactive artificial muscles. This could have great benefit to the growing field of soft robotic wearable assistive devices for people who are disabled or elderly. The growing topic of soft electroadhesion is also likely to benefit. Much work is currently underway to develop morphing structures that can also electrostatically grip and manipulate delicate objects (5), and ISW materials may enable new gripping structures and enhanced sensing functionality. By demonstrating an attractive combination of active (via electrostatically induced vibration) and passive (by dirt-repelling surface coatings) self-cleaning, this work also hints at future applications in active surfaces that clean themselves, either for aesthetics or for function. For example, wall-climbing robots that employ electroadhesion are currently limited to clean surfaces and dust-free environments (6), and developments deriving from the ISW could liberate them from these constraints. It would also be extremely interesting to develop the
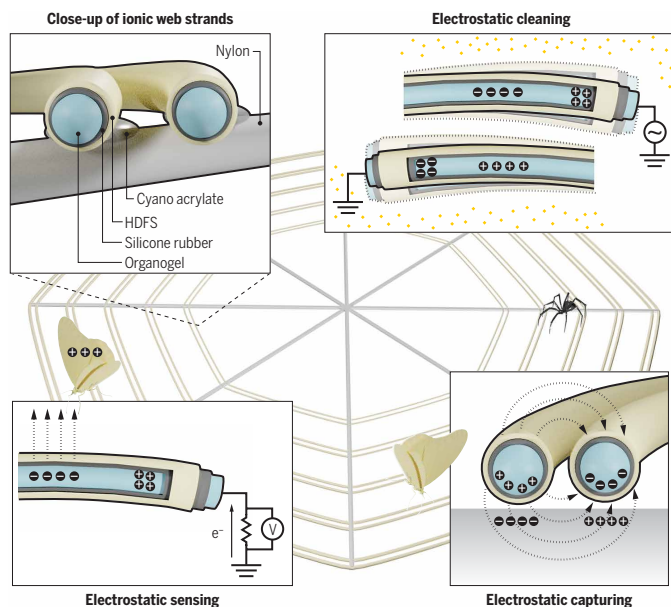

Fig. 1. The ISW. Conductive and compliant web fibers are made from ionic organogel encapsulated in silicone elastomer and coated with a low surface energy material [(heptadecafluoro-1,1,2,2-tetrahydrodecyl) trichlorosilane, HDFS]. The ISWs mimic the natural web and exhibit capabilities of object sensing and capture and hybrid self-cleaning.

Engineering Mathematics and Bristol Robotics Laboratory, University of Bristol, BS3 1NJ Bristol, UK. Email: jonathan.rossiter@bristol.ac.uk

spider analogy further, potentially seeing how spiders could work with the ISW in their natural environments, providing new insights into biology.

The ISWs presented are not without limitation. Improving the robustness of the web fibers under repeated stretching is a challenge, and the capability of the web to detect proximity of noncharged objects has yet to be demonstrated, although both will doubtless be addressed by the team and also by other scientists. The ISW can be seen as a generic technology that is applicable well beyond the mimicry of arachnid webs, and it remains to be seen how far these materials can be developed and adopted across soft robotics. Notwithstanding, the contribution of this work by Lee and colleagues to the fields of electrostatic actuation and controlled soft gripper is noteworthy and exciting.

REFERENCES

1. D. A. Parry, R. H. J. Brown, The hydraulic mechanism of the spider leg. *J. Exp. Biol.* **36**, 423–433 (1959).
2. H. Elettro, S. Neukirch, F. Vollrath, A. Antkowiak, In-drop capillary spooling of spider capture thread inspires hybrid fibers with mixed solid–liquid mechanical properties. *Proc. Natl. Acad. Sci. U.S.A.* **113**, 6143–6147 (2016).
3. Y. Lee, W. J. Song, Y. Jung, H. Yoo, M.-Y. Kim, H.-Y. Kim, J.-Y. Sun, Ionic spiderwebs. *Sci. Robot.* **5**, eaaz5405 (2020).
4. Y. Wu, D. U. Shah, C. Liu, Z. Yu, J. Liu, X. Ren, M. J. Rowland, C. Abell, M. H. Ramage, O. A. Scherman, Bioinspired supramolecular fibers drawn from a multiphase self-assembled hydrogel. *Proc. Natl. Acad. Sci. U.S.A.* **114**, 8163–8168 (2017).
5. J. Guo, J. Leng, J. Rossiter, Electroadhesion technologies for robotics: A comprehensive review. *IEEE T. Robot.* **36**, 313–327 (2020).
6. G. Gu, J. Zou, R. Zhao, X. Zhao, X. Zhu, Soft wall-climbing robots. *Sci. Robot.* **3**, eaat2874 (2018).

Science Robotics

Spinning artificial spiderwebs

Jonathan Rossiter

ARTICLE TOOLS	http://robotics.sciencemag.org/content/5/44/eabd0290
REFERENCES	This article cites 6 articles, 3 of which you can access for free http://robotics.sciencemag.org/content/5/44/eabd0290#BIBL
PERMISSIONS	http://www.sciencemag.org/help/reprints-and-permissions

SOFT ROBOTS

Ionic spiderwebs

Younghoon Lee[1]*, Won Jun Song[1]*, Yeonsu Jung[2], Hyunjae Yoo[1], Man-Yong Kim[3],
Ho-Young Kim[2]†, Jeong-Yun Sun[1,4]†

Spiders use adhesive, stretchable, and translucent webs to capture their prey. However, sustaining the capturing capability of these webs can be challenging because the webs inevitably invite contamination, thus reducing its adhesion force. To overcome these challenges, spiders have developed strategies of using webs to sense prey and clean contaminants. Here, we emulate the capturing strategies of a spider with a single pair of ionic threads based on electrostatics. Our ionic spiderwebs completed consecutive missions of cleaning contamination on itself, sensing approaching targets, capturing those targets, and releasing them. The ionic spiderwebs demonstrate the importance of learning from nature and push the boundaries of soft robotics in an attempt to combine mutually complementary functions into a single unit with a simple structure.

INTRODUCTION

Soft robots made of compliant materials are expected to flexibly handle unpredictable and irregular tasks based on their deformable bodies (1). With the advent of soft robots, individual components, such as soft sensors and actuators, have been actively researched (2–5). However, for soft robots to fully achieve their potential, each complementary component is required to be combined into a single robotic system (1, 6). Thus far, attempts have been made to combine diverse components, but achieving complementary interactions in a single system still remains a challenge (7–9). In contrast, biological systems successfully combine mutually complementary functions even in simple structures. For instance, spiders spin adhesive, stretchable, and translucent capture threads on strong structural threads used as a framework (10–13). The adhesive coating on the capture thread enables spiders to capture their prey (12–14). The translucent feature of capture thread allows for passive camouflage in all backgrounds (12, 13, 15). The stretchability of capture thread helps it to be compliant in various situations (12–14). However, the adhesive coating on capture thread inevitably invites contamination of the web (12). Because contamination deteriorates the capturing capability of webs, spiders (i.e., *Cyclosa japonica*) use unique strategies to minimize and eliminate such contamination (16, 17). Spiders build minimal webs and then wait for prey to come into contact with these webs (12, 13). After sensing vibrations of the web caused by the contact, spiders wrap the weakly caught prey with additional thread to supplement the adhesion force of the existing web (12, 13, 18–21). Thus, their sensing strategy not only prevents prey from escaping but also helps to minimize contamination by allowing the spiders to build minimal webs. Furthermore, spiders pull and rapidly release their webs in a manner similar to a slingshot, causing the contaminants on webs to bounce off by inertia force, thus recovering the capturing capability of the webs (Fig. 1B and movie S1). In this regard, spiders

can sense and clean using their webs alone, and these functions act synergistically to capture prey.

For the purpose of securing synergistic activity in a simple structure, the components should have similar operation mechanisms. One option that could meet this challenge is electrostatics, where capturing, sensing, and cleaning can be realized using only dielectric elastomers and soft electrodes. They can also be controlled quickly and accurately using an electrical circuit. Thus, adopting electrostatics might allow a simple structure to perform complementary functions and generate synergy (Fig. 1, F to H).

In this article, we emulate the capturing strategies of spiders based on electrostatics in ionic spiderwebs (ISWs) (Fig. 1, A and C; fig. S1; and Movie 1). An ISW was fabricated with ionically conductive and stretchable organogel encapsulated with silicone rubber to form a strand shape (Fig. 1D and figs. S2 and S3) (22–24). The organogel consists of covalently cross-linked polyacrylamide (PAAm) chains and ethylene glycol (EG) dissolving lithium chloride (LiCl) (Fig. 1E). Plasma etching and (heptadecafluoro-1,1,2,2-tetrahydrodecyl) trichlorosilane (HDFS) treatment of the silicone rubber markedly boosted cleaning capability and prevented evaporation of the organogel, which enhanced the durability of ISWs (fig. S4) (2, 25). In addition, similar to the structural thread of spiderwebs, nylon thread was used as the framework for ISWs to reinforce their mechanical properties (figs. S5 and S6 and table S1) (10–13).

RESULTS

Capturing by electrostatic adhesion

Spiders firmly capture various types of prey using their adhesive and stretchable webs. To emulate the capturing capability of these webs, electrostatic adhesion capturing was realized through the mechanism shown in Fig. 2 (A to D) (26, 27). In the OFF-state ($V_{applied} = 0$), the two threads remain separated (Fig. 2A). When a high voltage was applied, the ions were aligned along the organogel/silicone rubber interface of each thread, resulting in Maxwell stress between the threads (Fig. 2B) (3). As the threads moved closer, generation of a stronger electric field led to polarization in a target. The charge induced by polarization was attracted by the external electric field, and electrostatic adhesion occurred between the ISW and the target (Fig. 2C). Electrochemical reactions at the interface between an organogel and the metal electrode can be an issue (3). However, the electrostatic adhesion is based on a capacitive system. This lowers

[1]Department of Materials Science and Engineering, Seoul National University, 1 Gwanak-ro, Gwanak-gu, Seoul 08826, South Korea. [2]Department of Mechanical and Aerospace Engineering, Seoul National University, 1 Gwanak-ro, Gwanak-gu, Seoul 08826, South Korea. [3]Eumam Middle School, 147 Chilgeori-ro, Eumam-myeon, Seosan-si, Chungcheongnam-do 31936, South Korea. [4]Research Institute of Advanced Materials (RIAM), Seoul National University 1 Gwanak-ro, Gwanak-gu, Seoul 08826, South Korea.
*These authors contributed equally to this work.
†Corresponding author. Email: hyk@snu.ac.kr (H.-Y.K.); jysun@snu.ac.kr (J.-Y.S.)
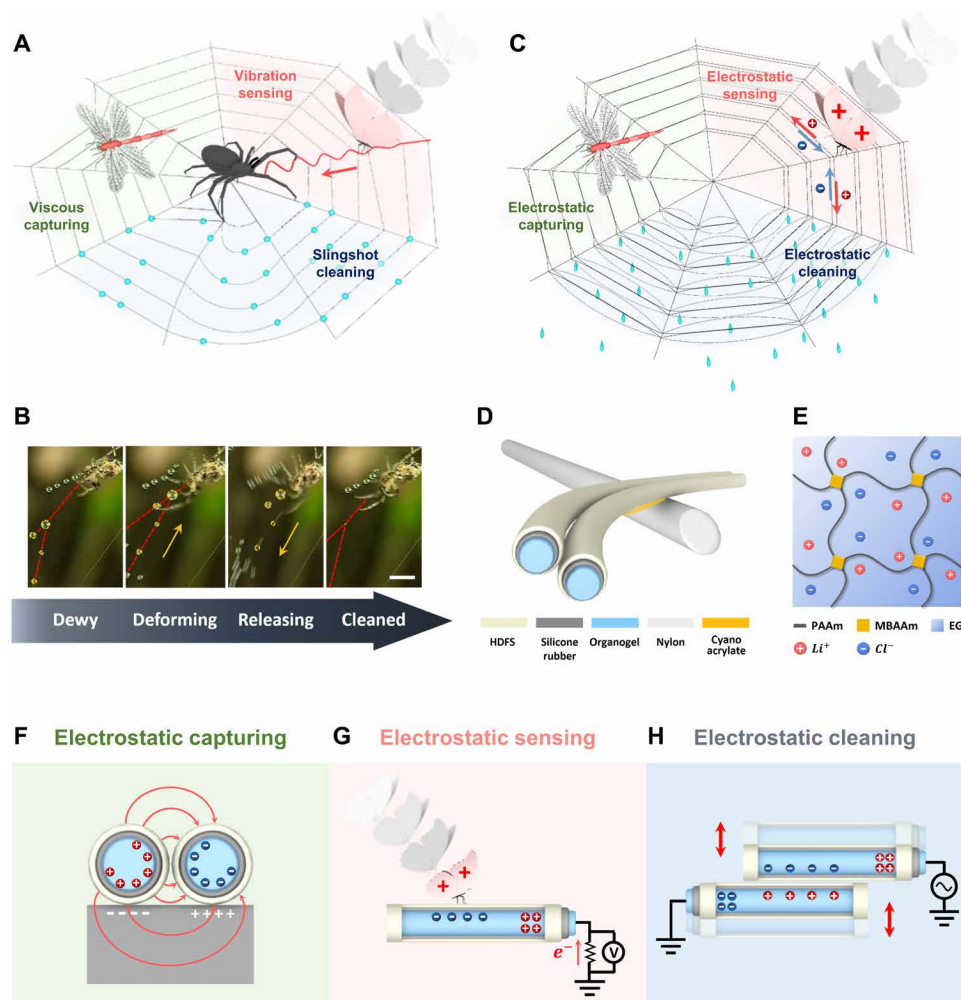
Movie 1. Summary of ISWs.

concerns about possible electrochemical reactions except for those caused by minimal leakage current, which was less than 2.3 nA/cm (see figs. S7 and S8 and the Supplementary Materials for details) (*3*). Although unwanted electrochemical reactions may be negligible, the ISWs can undergo breakdown if the electric field across dielectrics exceeds the dielectric strength of silicone rubber (50 to 100 kV/mm) (*9*). To address this safety issue, the leakage current was continuously measured to allow for immediate shut down of the applied voltage when a sudden increase in leakage current was sensed (see figs. S9 and S10 and the Supplementary Materials for details). To consolidate the working mechanism, the method of image charges was used to derive a mathematical expression for determining the electrostatic adhesion force exerted on a target, and the potential distribution was acquired, as shown in Fig. 2D (see fig. S11 and the Supplementary Materials for details).

To obtain a reproducible measurement of the electrostatic adhesion force, a universal testing machine with a custom acrylic holder was used (see Materials and Methods and movie S2 for details). As the applied voltage increased from 2 to 9 kV, the adhesion force per unit area improved from 0.1 to 0.3 kPa and 0.2 to 1.1 kPa when the target was poly(methyl methacrylate) (PMMA) and aluminum, respectively (Fig. 2E). The adhesion force was investigated with a variety of target materials—such as metals, ceramics, polymers, and natural materials—under a constant applied voltage of 5 kV (Fig. 2F). The highest adhesion force of 0.9 kPa was measured for metals, which have the highest dielectric constant, followed by ceramics (0.7 kPa) and polymers (0.25 kPa). This was because the higher the dielectric constant of the targets, the larger the polarization in the target under the same electric field. The conductivity of the organogel can be controlled by ion concentration. Figure 2G shows the effects of LiCl concentrations ranging from 0.15 mM to 1.5 M on the adhesion force. Ion concentration in the gel did not influence the adhesion force. The forces generated by electrostatic adhesion were investigated at varying tilt angles (Fig. 2H). The adhesion force increased by up to 6.5-fold when the ISW was tilted 80° from the horizontal, suggesting that ISWs can achieve substantial strength when tilted at a large angle (*28*, *29*). All components of the ISW are made of soft materials and can therefore be stretched. When a 50% strain was applied, adhesion force increased by 37%, as shown in Fig. 2I. A decrease in thickness of the silicone rubbers caused by stretching led the gels in a pair of ISWs to be closer to each other. This contributed to the generation of a stronger electric field, thus enhancing the electrostatic adhesion
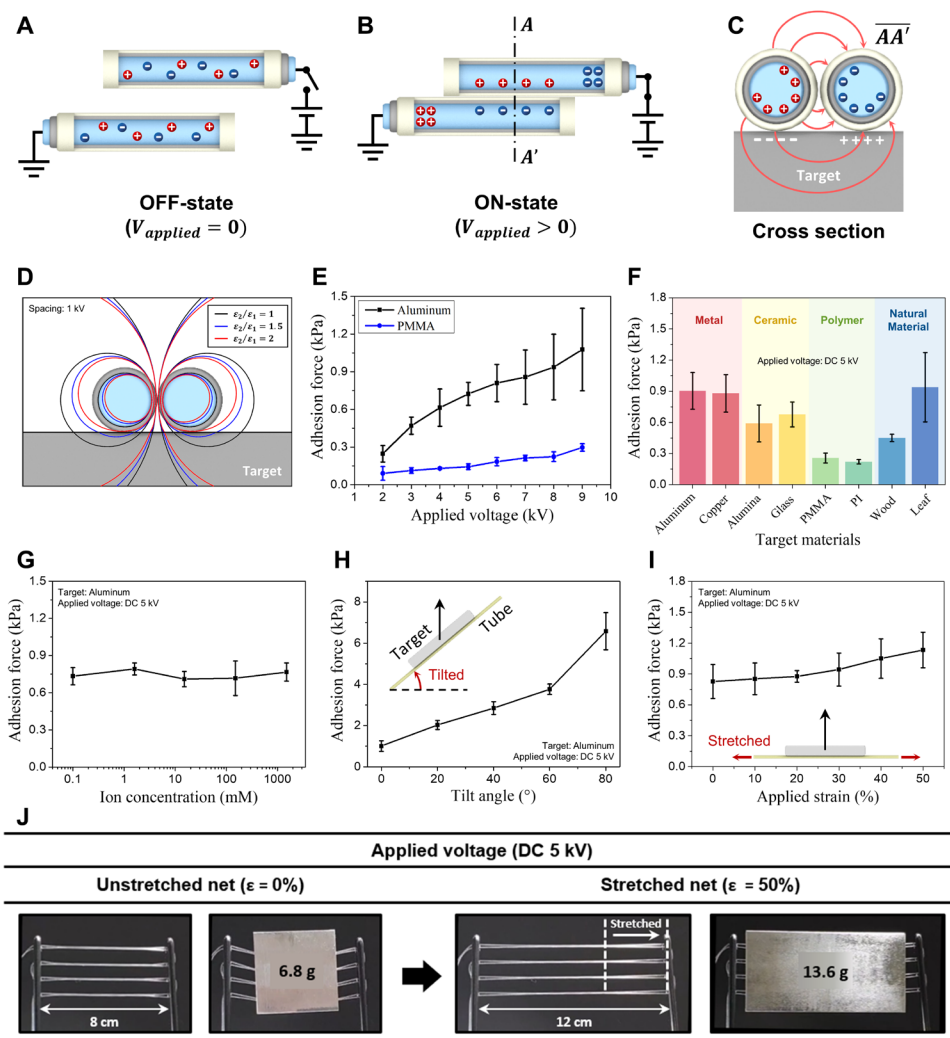

Fig. 1. Working principle of ISWs. (**A**) Spiders can sense and clean using their webs alone, and these functions act synergistically to capture their prey. (**B**) A spider removing dew drops from its web with slingshot cleaning. Scale bar, 3 mm. (**C**) ISWs emulating the capturing strategies of a spider. (**D**) Schematic illustration describing the structural design of a fabricated ISW. (**E**) Chemical structures of an ionically conductive organogel consisting of EG dissolving LiCl and PAAm chains cross-linked by MBAAm. (**F** to **H**) Simplified working mechanisms of electrostatic adhesion capturing, electrostatic induction sensing, and electrostatic vibration cleaning of ISWs.

Fig. 2. Capturing by electrostatic adhesion. (**A** to **C**) Schematic diagrams illustrating the working mechanism of electrostatic adhesion capturing in the OFF-state ($V_{applied} = 0$) (A) and ON-state ($V_{applied} > 0$) (B) with a cross-sectional view (C). The electric field generated by the potential difference between a pair of ISWs induces polarization in a target, leading to electrostatic adhesion capture. (**D**) Calculated potential distribution in ISWs and a target. (**E** to **I**) Adhesion force was investigated as a function of applied voltages (E), target materials (F), ion concentrations in the organogel (G), tilt angle (H), and applied strain (I). (**J**) Four pairs of ISWs capturing a 6.8-g aluminum plate. When 50% strain was applied, the ISWs captured a 13.6-g aluminum plate. Error bars in the figures represent SD ($n = 5$).

of dust can accelerate contamination (see Fig. 3A and movie S4 and Materials and Methods for details), and the electrostatic adhesion force of an ISW in the ON-state was substantially reduced to 1.8% after 50 s. Meanwhile, an ISW in the OFF-state still maintained 58.5% of its initial adhesion force because an ISW in the OFF-state was less contaminated compared with an ISW in the ON-state as shown in magnified images (Fig. 3, B and C).

To minimize contamination, spiders use a sensing strategy that allows them to build minimal webs. Inspired by this strategy, ISWs were equipped with a sensing capability that allowed them to turn on electrostatic adhesion only when a target is nearby. In this way, ISWs can minimize contamination by reducing the operating time of electrostatic adhesion. As described in Fig. 3 (D and E), making contact with the surroundings can charge the target through contact electrification (*30–32*). Approach of a charged target induces a voltage in the ISWs. Thus, measuring the voltage across an external load allows the relative distance between the ISW and the target to be measured. A target with no surface charge cannot be sensed. However, approaching targets can be sensed in most cases because they will be charged not only when they come into contact with other types of materials—including solids, liquids, and vapors—but also when they come into contact with the same type of material they are made of (*33–36*). Meanwhile, static objects around an ISW do not affect its sensing capability, because voltage is induced only when objects move (see figs. S12 and S13 and the Supplementary Materials for details). Because electrostatic induction sensing converts the mechanical energy of a target to an elec-

force. To demonstrate capturing capability, four pairs of ISWs were fixed at 1-cm intervals in a zigzag pattern and tilted approximately 80° relative to the horizontal (Fig. 2J and movie S3). Because of the simple structure, 0.2 g of ISWs was able to capture 6.8 g of an aluminum plate. The ISWs readily expanded to 50% of strain in the longitudinal direction and were able to capture a heavier target (13.6 g). Because the stretched ISWs were under tension, they showed less deflection when capturing a target.

Sensing by electrostatic induction

One of the major concerns for spiders capturing prey is contamination of webs due to their strong adhesion force. Similar to spiderwebs, the adhesion force of an ISW can attract undesirable contaminants. For example, an air circulation system that scatters dense particles

trical signal, it has the advantage of negligible power consumption compared with existing proximity sensing technologies (*37*).

A pushing tester was used to reproducibly control the distance and approaching speed of the targets (Fig. 3F). Static charges were created on the surface of a target by rubbing a glass with various charging materials (see Materials and Methods for details). The sensing capability was tested with various gap distances (d), ranging from 0.5 to 1.5 cm, under a sinusoidal wave of 1 Hz (Fig. 3G). These measured voltages closely traced the position of the target. In addition, contact of a target with an ISW could also be sensed (fig. S14). However, because switching from sensing mode to capturing mode takes time, ISWs are required to sense the approach of a target before contact occurs and then turn on electrostatic adhesion in advance. To obtain the highest sensitivity, the induced voltages were measured
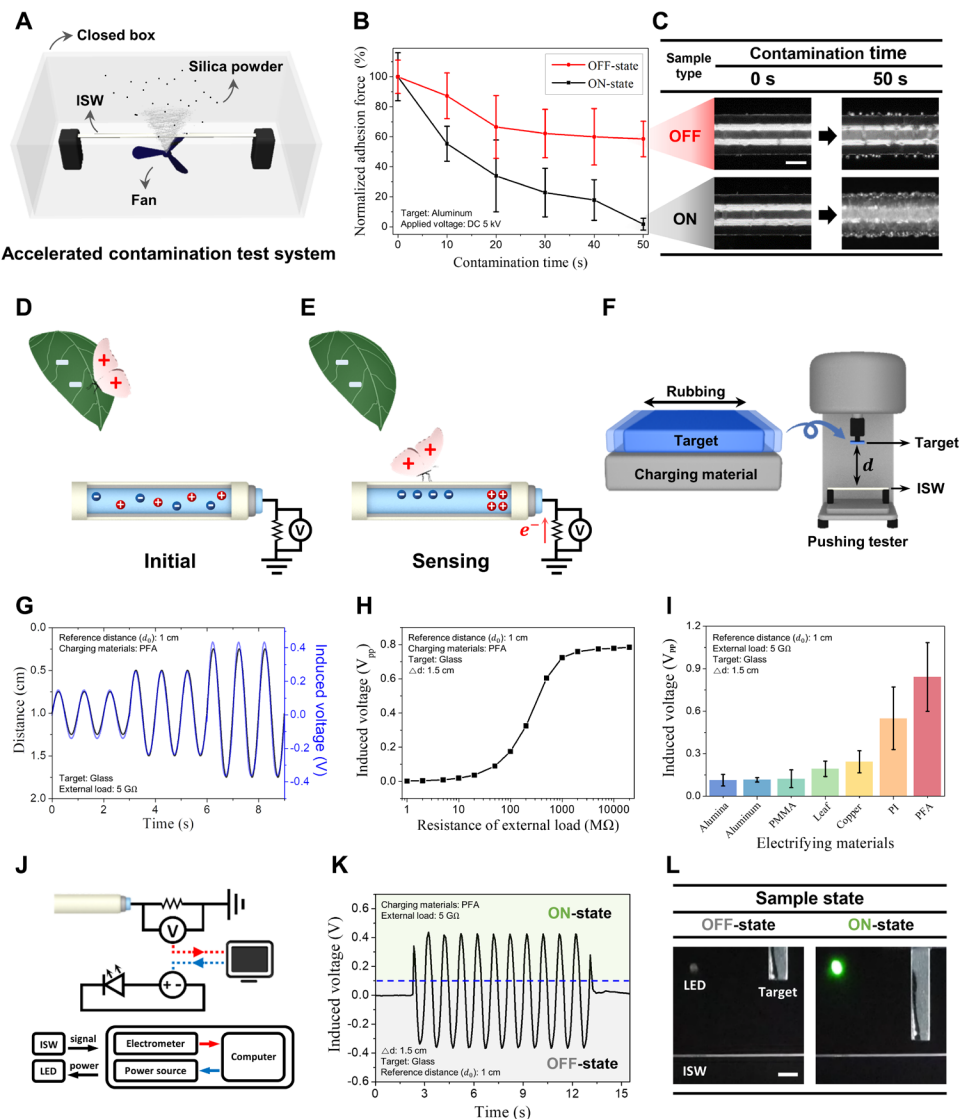
Fig. 3. Sensing by an electrostatic induction. (**A**) Air circulation system that scatters dense dust to accelerate contamination. (**B**) Normalized electrostatic adhesion forces of ISWs after exposure to contaminants in the ON-state and OFF-state. (**C**) Contaminated surfaces of ISWs. Scale bar, 150 μm. (**D** and **E**) Schematic diagrams showing the working mechanism of electrostatic induction sensing. (**F**) A pushing tester providing consistent control of the moving speed and gap distance for electrostatic induction sensing. (**G**) Induced voltage in ISWs is investigated as a function of the gap distance between an ISW and a target. (**H** and **I**) Peak-to-peak voltages induced by a glass target were measured using an external load with resistance ranging from 1 megohm to 20 gigohms (H) and various charging materials (I). (**J**) A block diagram showing how the ISW senses the approach of a target and then interacts with a preprogrammed computer. (**K** and **L**) A green LED was turned on when the induced voltage exceeded a threshold voltage (0.1 V). Scale bar, 5 mm. Error bars represent SD ($n = 5$).

with various external loads. The induced voltage was enhanced with increasing resistance of the external load under various target approach speeds of a target (Fig. 3H and fig. S15). The induced voltage was measured when the target was charged by various materials, such as alumina, aluminum, PMMA, leaf, copper, polyimide, and perfluoro-alkoxy alkane (PFA) (Fig. 3I). Perceptible values of 0.11 V_{pp} were measured even when the target was charged with alumina, which is known to have an electron affinity similar to that of the target (*38*). A circuit was fabricated to demonstrate how an ISW could sense an

approaching target and then turn on a power source using a preprogrammed computer (Fig. 3J). When the induced voltage exceeded a threshold voltage of 0.1 V for sensing, the computer allowed the power source to operate. As shown in Fig. 3 (K and L) (as well as in movie S5), a green light-emitting diode (LED) was turned on when an ISW sensed the approach of a target.

Cleaning by electrostatic vibration
A spider can pull and release its web in a manner similar to a slingshot to clean contamination. An ISW emulates a spider's cleaning strategy to recover its capturing capability by eliminating contaminants. As shown in Fig. 4 (A to C), vibration cleaning based on the electrostatic attraction between ISWs was proposed. In the initial state ($V_{applied} = 0$), the two threads are separated (Fig. 4A). When a high voltage is applied, the threads attract each other by Maxwell stress (Fig. 4B) (*3*, *39*). As the applied voltage approaches zero again, the threads are released (Fig. 4C). Thus, alternating attraction and release caused a vibration in the ISW. When the vibration frequency matched the resonant frequency of the ISW, the vibration amplitude was maximized and contaminants could bounce off by their inertia.

The amplitude of electrostatic vibration was investigated using different frequencies of applied voltage ranging from 20 to 116 Hz, as shown in Fig. 4D (see movie S6 and Materials and Methods for details). When the length of the threads was 6 cm, resonance occurred at 46 Hz (mode number, $n = 1$) and 92 Hz ($n = 2$). When the length of the threads decreased from 6 to 3 cm, the resonant frequencies of the first and second mode increased from 46 to 97 Hz and from 92 to 195 Hz, respectively, as shown in Fig. 4E. Therefore, to clean ISWs of various lengths, it is necessary to sweep the entire frequency range containing all resonant frequencies. To verify the cleaning effect by vibration, recovery of the adhesion force was investigated after the surface of an ISW was sufficiently contaminated (Fig. 4F). During 60 s of vibration cleaning including three cycles of frequency sweeps, the adhesion force was restored to 98.7% of the initial force. Insets show the surface of the ISW before and after vibration cleaning.

Compared with other contaminants, a droplet of water is more difficult to remove due to its high surface tension. To clean a droplet of water by electrostatic vibration, the surface of the ISW was physically and chemically treated (see Materials and Methods for details).
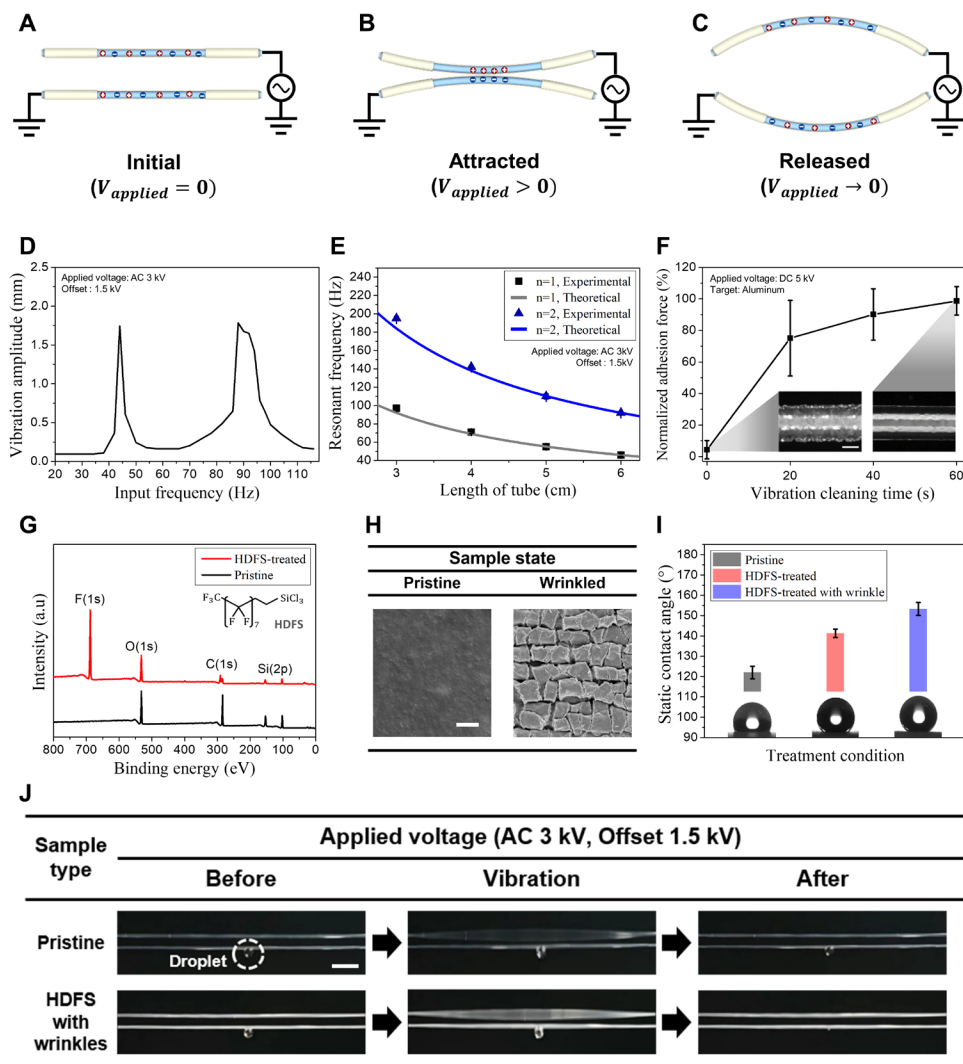
Fig. 4. Cleaning by electrostatic vibration. (**A** to **C**) Schematic diagrams showing the working mechanism of electrostatic vibration cleaning in the initial (A), attracted ($V_{applied} > 0$) (B), and released ($V_{applied} \rightarrow 0$) (C) states. (**D**) To determine a resonant frequency of the ISW, the frequency of the applied voltage was swept from 20 to 116 Hz. (**E**) Resonant frequencies were measured using different length threads. (**F**) The adhesion force of a contaminated ISW was recovered as vibration cleaning removed contaminants. Scale bar, 300 μm. (**G**) An x-ray photoelectron spectrometer (XPS) was used to characterize the HDFS on surfaces of ISWs. (**H**) Wrinkles were formed on the surface of ISWs to enhance their hydrophobicity. Scale bar, 1 μm. (**I**) Static contact angles depending on surface treatment. (**J**) Cleaning capabilities of pristine and surface-treated ISWs. A droplet hanging on surface-treated ISWs was removed by vibration, whereas a droplet remained on the pristine ISWs. Scale bar, 5 mm. Error bars represent SDs [in (F), $n = 5$; in (I), $n = 3$].

frequency sweep of the applied voltage. Droplets of water were initially suspended from each ISW. A droplet on a surface-treated ISW was cleaned during the vibration, whereas a droplet on a pristine ISW was not cleaned off (movie S7).

Ionic spiderwebs

An ISW was fabricated in the form of an orb web, as shown in Fig. 5A. A pair of threads was fixed on nylon threads as a framework (Fig. 5B). The distance between the pairs was 1 cm (d_o), and the distance between threads in a pair was 3 mm (d_i). The ISW exhibits passive camouflage in diverse environments (such as a forest, fallen leaves, a brick wall, and the floor of a building) because it is transparent and thin, as shown in Fig. 5C. In an attempt to enhance the adhesion force, the ISW was tilted to 80° from the horizontal. In the initial state, the ISW was contaminated with dust, such as polyurethane particles (Fig. 5D, i). During cleaning, a frequency of the applied voltage was swept from 30 to 60 Hz for 200 s, and the dust that covered the ISW was notably cleaned (Fig. 5D, ii). After the cleaning, the ISW was turned to sensing mode with no applied voltage. When an approaching target caused the induced voltage to exceed the threshold voltage of 1 V, the ISW was rapidly converted to capturing mode (Fig. 5D, iii). Various types of materials—such as a leaf (0.4 g), PMMA (3.1 g), glass (8.5 g), and aluminum (11 g)—were tightly captured by the electrostatic adhesion of the ISW (Fig. 5D, iv). After performing the mission, the targets were released by application of 30 Hz of AC voltage to the ISW (Fig. 5D, v). The entire continuous process is shown in movie S8.

DISCUSSION

Inspired by how spiders capture their prey in spiderwebs, we emulate the abilities to capture, sense, and clean in our ISWs. Through electrostatics, all of these features were realized with a single pair of threads consisting of ionically conductive organogel encapsulated by a silicone rubber. The ISWs developed in this study robustly captured various types of targets, including an aluminum with a 68-fold greater mass. An ISW's stretchability enhanced its capturing capability by reducing the thickness of the silicone rubber. The sensing capability of the ISW allowed it to turn on electrostatic adhesion only when a target was nearby to avoid undesirable contamination. This contributed to the maintenance of the adhesion force, which was 32.5 times higher than that of an ISW without sensing capability. The cleaning
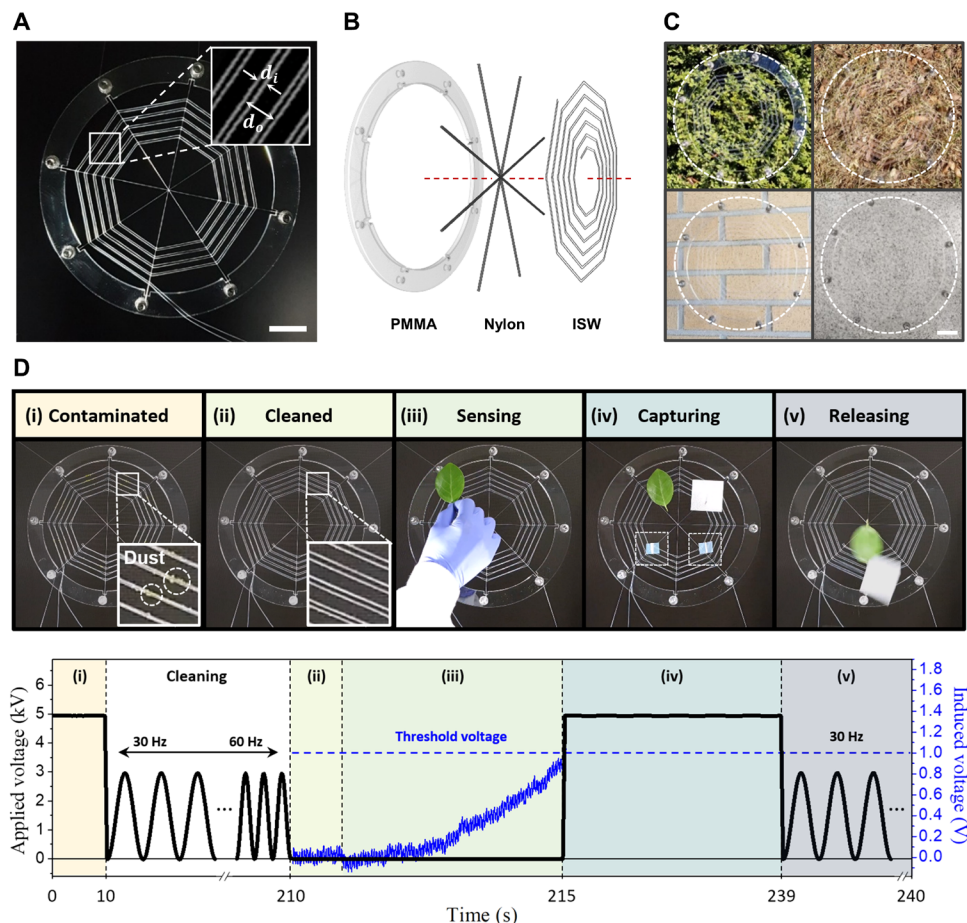
Perfluorination of ISWs using HDFS can lower surface energy (*2, 25*). X-ray photoelectron spectroscopy (XPS) was implemented to characterize the functionalized ISWs (Fig. 4G). The spectral peak of fluorine 1s orbital was observed, confirming the presence of fluorine on the ISW after HDFS treatment. To improve the hydrophobicity of ISWs, microwrinkles were formed by air plasma treatment of prestretched ISWs (Fig. 4H) (*40, 41*). Through HDFS treatment, the static contact angle of water was improved from 122° to 141.3°. Microscale wrinkles with a HDFS treatment maximized the static contact angle from 141.3° to 153.3° (Fig. 4I). Figure 4J shows the cleaning capabilities of pristine and surface-treated ISWs using a

Fig. 5. Ionic spiderwebs. (**A** and **B**) ISW woven in the form of an orb web (A) and exploded view (B). Scale bar, 3 cm. (**C**) ISWs are passively camouflaged in a variety of environment such as a forest, fallen leaves, a brick wall, and the floor of a building. Scale bar, 4 cm. (**D**) An ISW is initially covered with dust (i). The dust is removed (ii). The ISW senses the approach of a target and then converted to capturing mode (iii). Leaf, PMMA, glass, and aluminum were sequentially captured by the ISW (iv). The targets were released from the ISW (v).

(Sigma, L4408) was used as an ionic charge carrier. Lithium phenyl-2,4,6-trimethylbenzoylphosphinate (LAP; Sigma, 900889) was used as a photo initiator. Silicone tubes with inner diameters of 500 μm and outer diameters of 600 μm (Axel, 1-8194-05, https://axel-search-e.as-1.co.jp/asone/global/g/NC2006025965/) were used as dielectrics in ISWs. HDFS (JSI Silicone Co, H5060.1) was used as surface fluorination agent. Ethyl cyanoacrylate (Henkel, Loctite 406) and a primer (Henkel, Loctite SF770) were used to bond ISWs to nylon threads with a diameter of 0.52 mm (Ourix, Shock Leader) (*42*). Platinum electrodes were used to connect the organogel with electrical circuits.

Preparation of organogel precursor solution
Unless otherwise specified, the ionic organogel was synthesized by dissolving AAm and LiCl in EG. The molar concentrations of the AAm and LiCl solutions were 3.5 and 1.5 M, respectively. MBAAm [0.124 weight % (wt %)] and LAP (0.012 wt %) with respect to the weight of AAm were added.

Fabrication of ISWs
Unless otherwise specified, surface etching of prestrained (150%) silicone tubes was conducted using an air plasma processing system (FEMTO SCIENCE, COVANCE-1MPR) under conditions of 200 W, 1 hour, and 15 sccm (standard cubic centimeters per minute). The silicone tubes were immersed in a solution of HDFS and hexane mixed at a ratio of 1:500. Self-assembled monolayer formation took place for 20 min. Treated ISWs were then washed with hexane for 10 min. Organogel precursor solution was injected into surface-treated silicone tubes, followed by 365-nm ultraviolet irradiation (CL-1000L, UVP) under inert conditions for 5 min. Pretreatment using a primer was carried out on ISWs at the intersection with nylon thread to promote wetting of the adhesive (*42*). A pair of ISWs was bonded to nylon threads using ethyl cyanoacrylate. A stereomicroscope (Stereo Discovery V12, Zeiss) was used to observe the fabricated ISW.

Characterization and measurement of electrostatic adhesion capturing
For all measurements of electrostatic adhesion force, a universal testing machine (Instron, 3343) with a static load cell (Instron, 2530-50N) was used at a fixed receding rate of 3 mm/min. Targets and ISWs were fixed in place with a custom acrylic holder. Unless otherwise specified, the adhesion force of ISWs was measured using aluminum as a target under 5 kV of applied voltage. ISWs were connected to a power source via Pt electrodes. A function generator

capability of the ISW, which was reinforced by surface modifications, ensured the removal of inevitable contaminants. With electrostatic vibration cleaning, an ISW was able to recover its adhesion force up to 98.7%. Our approach is potentially applicable to other existing robotic components based on electrostatics, such as electrostatic adhesion grippers, dielectric elastomer actuators, and capacitive tactile sensors. They are expected to equip additional functionalities and broaden the scope of applications potentially without major structural changes. The proposed ISWs offer a design principle for soft robots that can achieve complementary interactions between each robotic component by emulating synergic functions of nature.

MATERIALS AND METHODS
Materials and specimen preparation
Unless otherwise specified, ISWs were fabricated using a PAAm organogel containing LiCl. Acrylamide (AAm; Sigma, A8887) and *N,N*-methylenebisacrylamide (MBAAm; Sigma, M7279) were used as monomers and cross-linkers for the organogel, respectively. EG (Dae-Jung, 4026-4404) was used as a liquid constituent. LiCl

(Agilent, 33612A) with a high-voltage amplifier (Trek, 30/20A) was used as a power source for electrostatic adhesion capturing. The leakage current was measured using a multimeter (Agilent, 34461A). Adhesion force per unit area was calculated in a projection area in which the sample and target met.

Demonstration of stretchable electrostatic adhesion net
Four pairs of ISWs were fixed parallel to the holders. The gaps between each pair were 1 cm, whereas the gap between threads in a pair was 3 mm. The ISW was manually stretched from 8 to 12 cm under the applied voltage. To release the target, 3 kV of AC voltage with an offset of 1.5 kV and a frequency of 30 Hz were applied to the ISW. The targets consisted of aluminum at sizes of 5 cm by 5 cm by 0.1 cm (6.8 g) and 10 cm by 5 cm by 0.1 cm (13.6 g).

Test of contamination
Contamination was tested using a cubic-shaped acrylic system (1.73L). ISWs were set at the center of the system. Each ISW was kept under adhesion ON-state and OFF-state, respectively. Ten grams of silica powder with an average particle diameter of 50 μm was then scattered using a fan for 50 s, and adhesion force was measured every 10 s during this time. An inverted microscope (Olympus Korea, CKX41-A32PH standard) was used to observe contamination on the surface of the ISWs.

Characterization and measurement of electrostatic induction sensing
Unless otherwise indicated, ISWs were connected to an external load of 5 gigohms. An electrometer (Keithley, 6517A) was used to measure induced voltage across the external load. A pushing tester (Labworks, LW139.138-40) with a linear power amplifier (Labworks, PA-138) was used to provide vertical linear motion of the targets. A glass target was charged by rubbing with PFA. The targets moved in a sinusoidal pattern with a frequency of 1 Hz. The reference distance and amplitude were 1 and 0.75 cm, respectively. All measurements of electrostatic induction sensing were conducted in a Faraday cage to prevent ambient electrical noise (see fig. S16 and the Supplementary Materials for details). To show interactions with a computer, LabView (National Instruments) was used for programming.

Characterization and measurement of electrostatic vibration cleaning
A function generator (Agilent, 33612A) with a high-voltage amplifier (Trek, 30/20A) was used as a power source to provide sinusoidal high voltages. To measure the vibration amplitude of ISWs, a high-speed camera (Phantom, V611-32G-MAG) that could run up to 6242 frames per second was used. Contact angles of deionized water on ISW were measured with a contact angle analyzer (FEMTOFAB, Smart Drop) at room temperature. An x-ray photoelectron spectrometer (Kratos, AXIS-HSi) was used to characterize functionalized ISWs. A field-emission scanning electron microscope (Carl Zeiss, Sigma) was used to observe surface morphology of ISWs. To investigate cleaning capability of ISW, 10 g of silica powder and a 5-μl water droplet were used as contaminants. The frequency of the applied voltage was swept from 45 to 100 Hz for 20 s.

Recording of slingshot cleaning by a spider
The slingshot cleaning behavior of a *C. japonica* specimen was recorded in Galsan-dong, Seosan-si, Chungnam, South Korea.

SUPPLEMENTARY MATERIALS
robotics.sciencemag.org/cgi/content/full/5/44/eaaz5405/DC1
Supplementary Text
Fig. S1. ISWs emulating the optimized capturing strategies of spiders.
Fig. S2. Fabrication process of an ISW.
Fig. S3. Magnified image of an ISW.
Fig. S4. Anti-dehydration capability of ISWs under harsh conditions.
Fig. S5. Exploded view of orb spiderwebs.
Fig. S6. Stress-strain curve of tensile test.
Fig. S7. Equivalent circuit of electrostatic adhesion capturing.
Fig. S8. Leakage current of ISW.
Fig. S9. Breakdown voltages of ISW.
Fig. S10. Dielectric breakdown behavior of ISW.
Fig. S11. Problem definition for deriving mathematical expression of electrostatic adhesion force.
Fig. S12. Schematic describing the effect of static objects around the ISW.
Fig. S13. Experimental results describing the effect of static objects around the ISW.
Fig. S14. Induced voltage when a target contacts ISW.
Fig. S15. Induced voltages measured with various resistances of external loads and approaching speeds of a target.
Fig. S16. Demonstration of electrostatic induction sensing under practical conditions.
Table S1. Tensile mechanical properties of spiderwebs and ISWs.
Movie S1. Slingshot cleaning of spiders.
Movie S2. Measurement of electrostatic adhesion force.
Movie S3. Stretchable electrostatic adhesion net.
Movie S4. Test of contamination.
Movie S5. Sensing by electrostatic induction.
Movie S6. Measurement of vibration amplitude.
Movie S7. Cleaning by electrostatic vibration.
Movie S8. Ionic spiderwebs.
References (*43*–*45*)

REFERENCES AND NOTES
1. D. Rus, M. T. Tolley, Design, fabrication and control of soft robots. *Nature* **521**, 467–475 (2015).
2. Y. Lee, S. H. Cha, Y.-W. Kim, D. Choi, J.-Y. Sun, Transparent and attachable ionic communicators based on self-cleanable triboelectric nanogenerators. *Nat. Commun.* **9**, 1804 (2018).
3. C. Keplinger, J.-Y. Sun, C. C. Foo, P. Rothemund, G. M. Whitesides, Z. Suo, Stretchable, transparent, ionic conductors. *Science* **341**, 984–987 (2013).
4. C.-C. Kim, H.-H. Lee, K. H. Oh, J.-Y. Sun, Highly stretchable, transparent ionic touch panel. *Science* **353**, 682–687 (2016).
5. J.-Y. Sun, C. Keplinger, G. M. Whitesides, Z. Suo, Ionic skin. *Adv. Mater.* **26**, 7608–7614 (2014).
6. S. I. Rich, R. J. Wood, C. Majidi, Untethered soft robotics. *Nat. Electron.* **1**, 102–112 (2018).
7. D. Y. Kim, S. Choi, H. Cho, J.-Y. Sun, Electroactive soft photonic devices for the synesthetic perception of color and sound. *Adv. Mater.* **31**, e1804080 (2019).
8. C. Larson, B. Peele, S. Li, S. Robinson, M. Totaro, L. Beccai, B. Mazzolai, R. Shepherd, Highly stretchable electroluminescent skin for optical signaling and tactile sensing. *Science* **351**, 1071–1074 (2016).
9. J. Shintake, S. Rosset, B. Schubert, D. Floreano, H. Shea, Versatile soft grippers with intrinsic electroadhesion based on multifunctional polymer actuators. *Adv. Mater.* **28**, 231–238 (2016).
10. S. W. Cranford, A. Tarakanova, N. M. Pugno, M. J. Buehler, Nonlinear material behaviour of spider silk yields robust webs. *Nature* **482**, 72–76 (2012).
11. F. G. Omenetto, D. L. Kaplan, New opportunities for an ancient material. *Science* **329**, 528–531 (2010).
12. R. F. Foelix, *Biology of Spiders* (Georg Thieme Verlag, 1979).
13. T. A. Blackledge, M. Kuntner, I. Agnarsson, in *Advances in Insect Physiology* (Elsevier, 2011), vol. 41, pp. 175–262.
14. L. Römer, T. Scheibel, The elaborate structure of spider silk: Structure and function of a natural high performance fiber. *Prion* **2**, 154–161 (2008).
15. C. L. Craig, Orb-web visibility: The influence of insect flight behaviour and visual physiology on the evolution of web designs within the Araneoidea. *Anim. Behav.* **34**, 54–68 (1986).
16. W. M. Masters, H. Markl, Vibration signal transmission in spider orb webs. *Science* **213**, 363–365 (1981).
17. P. Fratzl, F. G. Barth, Biomaterial systems for mechanosensing and actuation. *Nature* **462**, 442–448 (2009).
18. T. Eisner, R. Alsop, G. Ettershank, Adhesiveness of spider silk. *Science* **146**, 1058–1061 (1964).

19. T. A. Blackledge, C. M. Eliason, Functionally independent components of prey capture are architecturally constrained in spider orb webs. *Biol. Lett.* **3**, 456–458 (2007).

20. W. M. Barrows, The reactions of an orb-weaving spider, *Epeira sclopetaria* Clerck, to rhythmic vibrations of its web. *Biol. Bull.* **29**, 316–332 (1915).

21. W. Nentwig, Why do only certain insects escape from a spider's web? *Oecologia* **53**, 412–417 (1982).

22. H.-R. Lee, C.-C. Kim, J.-Y. Sun, Stretchable ionics–A promising candidate for upcoming wearable devices. *Adv. Mater.* **30**, e1704403 (2018).

23. C. Yang, Z. Suo, Hydrogel ionotronics. *Nat. Rev. Mater.* **3**, 125–142 (2018).

24. H. Yuk, B. Lu, X. Zhao, Hydrogel bioelectronics. *Chem. Soc. Rev.* **48**, 1642–1667 (2019).

25. S. J. Clarson, M. J. Owen, S. D. Smith, M. Van Dyke, M. Brook, J. Mabry, *Progress in Silicones and Silicone-Modified Materials* (ACS Publications, 2013).

26. M. A. Graule, P. Chirarattananon, S. B. Fuller, N. T. Jafferis, K. Y. Ma, M. Spenko, R. Kornbluh, R. J. Wood, Perching and takeoff of a robotic insect on overhangs using switchable electrostatic adhesion. *Science* **352**, 978–982 (2016).

27. G. Gu, J. Zou, R. Zhao, X. Zhao, X. Zhu, Soft wall-climbing robots. *Sci. Robot.* **3**, eaat2874 (2018).

28. V. Cacucciolo, J. Shintake, H. Shea, in *2019 2nd IEEE International Conference on Soft Robotics (RoboSoft)* (IEEE, 2019), pp. 108–113.

29. J. W. Hutchinson, Z. Suo, in *Advances in Applied Mechanics* (Elsevier, 1991), vol. 29, pp. 63–191.

30. H. H. Zakon, Electric fields of flowers stimulate the sensory hairs of bumble bees. *Proc. Natl. Acad. Sci. U.S.A.* **113**, 7020–7021 (2016).

31. V. M. Ortega-Jimenez, R. Dudley, Spiderweb deformation induced by electrostatically charged insects. *Sci. Rep.* **3**, 2108 (2013).

32. F.-R. Fan, Z.-Q. Tian, Z. L. Wang, Flexible triboelectric generator. *Nano Energy* **1**, 328–334 (2012).

33. G. Xue, Y. Xu, T. Ding, J. Li, J. Yin, W. Fei, Y. Cao, J. Yu, L. Yuan, L. Gong, J. Chen, S. Deng, J. Zhou, W. Guo, Water-evaporation-induced electricity with nanostructured carbon materials. *Nat. Nanotechnol.* **12**, 317–321 (2017).

34. J. Nie, Z. Wang, Z. Ren, S. Li, X. Chen, Z. L. Wang, Power generation from the interaction of a liquid droplet and a liquid membrane. *Nat. Commun.* **10**, 2264 (2019).

35. H. T. Baytekin, A. Z. Patashinski, M. Branicki, B. Baytekin, S. Soh, B. A. Grzybowski, The mosaic of surface charge in contact electrification. *Science* **333**, 308–312 (2011).

36. M. M. Apodaca, P. J. Wesson, K. J. M. Bishop, M. A. Ratner, B. A. Grzybowski, Contact electrification between identical materials. *Angew. Chem. Int. Ed.* **49**, 946–949 (2010).

37. M. S. Sarwar, Y. Dobashi, C. Preston, J. K. M. Wyss, S. Mirabbasi, J. D. W. Madden, Bend, stretch, and touch: Locating a finger on an actively deformed transparent sensor array. *Sci. Adv.* **3**, e1602200 (2017).

38. Y. J. Kim, J. Lee, S. Park, C. Park, C. Park, H.-J. Choi, Effect of the relative permittivity of oxides on the performance of triboelectric nanogenerators. *RSC Adv.* **7**, 49368–49373 (2017).

39. E. Acome, S. K. Mitchell, T. G. Morrissey, M. B. Emmett, C. Benjamin, M. King, M. Radakovitz, C. Keplinger, Hydraulically amplified self-healing electrostatic actuators with muscle-like performance. *Science* **359**, 61–65 (2018).

40. A. Tuteja, W. Choi, J. M. Mabry, G. H. McKinley, R. E. Cohen, Robust omniphobic surfaces. *Proc. Natl. Acad. Sci. U.S.A.* **105**, 18200–18205 (2008).

41. A. Marmur, The lotus effect: Superhydrophobicity and metastability. *Langmuir* **20**, 3517–3519 (2004).

42. D. Wirthl, R. Pichler, M. Drack, G. Kettlguber, R. Moser, R. Gerstmayr, F. Hartmann, E. Bradt, R. Kaltseis, C. M. Siket, S. E. Schausberger, S. Hild, S. Bauer, M. Kaltenbrunner, Instant tough bonding of hydrogels for soft machines and electronics. *Sci. Adv.* **3**, e1700053 (2017).

43. J. D. Jackson, *Classical Electrodynamics* (Wiley, 1975).

44. C. Chiang Foo, S. Cai, S. J. A. Koh, S. Bauer, Z. Suo, Model of dissipative dielectric elastomers. *J. Appl. Phys.* **111**, 034102 (2012).

45. N. M. Farhan, H. Vahedi Tafreshi, Universal expression for droplet–fiber detachment force. *J. Appl. Phys.* **124**, 075301 (2018).

Science Robotics

Ionic spiderwebs

Younghoon Lee, Won Jun Song, Yeonsu Jung, Hyunjae Yoo, Man-Yong Kim, Ho-Young Kim and Jeong-Yun Sun

ARTICLE TOOLS	http://robotics.sciencemag.org/content/5/44/eaaz5405
SUPPLEMENTARY MATERIALS	http://robotics.sciencemag.org/content/suppl/2020/07/13/5.44.eaaz5405.DC1
REFERENCES	This article cites 39 articles, 13 of which you can access for free http://robotics.sciencemag.org/content/5/44/eaaz5405#BIBL
PERMISSIONS	http://www.sciencemag.org/help/reprints-and-permissions

Science Robotics
AAAS

Supplementary Materials for

Ionic spiderwebs

Younghoon Lee, Won Jun Song, Yeonsu Jung, Hyunjae Yoo, Man-Yong Kim, Ho-Young Kim*, Jeong-Yun Sun*

*Corresponding author. Email: hyk@snu.ac.kr (H.-Y.K.); jysun@snu.ac.kr (J.-Y.S.)

The PDF file includes:

Other Supplementary Material for this manuscript includes the following:

Movie S3 (.mp4 format). Stretchable electrostatic adhesion net.
Movie S4 (.mp4 format). Test of contamination.
Movie S5 (.mp4 format). Sensing by electrostatic induction.
Movie S6 (.mp4 format). Measurement of vibration amplitude.
Movie S7 (.mp4 format). Cleaning by electrostatic vibration.
Movie S8 (.mp4 format). Ionic spiderwebs.

Supplementary Text

Mathematical model on electrostatic adhesion force of ISWs.

A mathematical expression was formulated to obtain the electrostatic adhesion force exerted on the target. When voltage is applied on the ISW, the electric field polarizes the target surface regardless of whether the target is a conductor or an insulator. The induced charge due to polarization is attracted by the external electric field. Since there is no free charges except in the interior of the ISW, the electric potential in the given domain, ϕ, must satisfy Laplace's equation,

$$\nabla^2 \phi = 0, \tag{1}$$

and the following boundary conditions: electric potential is fixed at the interface between interior organogel and silicone rubber, $\phi = 2\phi_0 = 5$ kV and $\phi = 0$ for the left and right threads, respectively; and electrostatic boundary conditions hold for each interface between two distinct materials with different dielectric constants (fig. S11).

An analytical solution satisfying Laplace's equation and all boundary conditions is not available because of the complicated geometry involved. Instead, a solution that partially and approximately satisfies these boundary conditions was used. First, the space filled with air was neglected and the upper domain was assumed to be filled with silicone rubber of relative permittivity, $\varepsilon_1 \approx 3$ ($y > 0$). Then, the method of image charges was used (*43*), in which several imaginary charges were placed in the domain and analyzed on how the resulting electric field calculated by the superposition principle matched the given conditions.

Line charges were placed in the domain as shown in Fig. S1B. λ, $-\lambda$, λ', and λ' were charge densities of the imaginary line charges located at positions $(-a, b)$, (a, b), $(-a, -b)$, and $(a, -b)$, respectively. Parameters λ, λ', a, and b were determined by applying boundary conditions. Throughout this section, the domain above the target ($y > 0$) was denoted by subscript $i = 1$ and that below the target surface ($y < 0$) by subscript $i = 2$. By placing four line charges perpendicular to the xy plane as shown in fig. S11B, the electric potential at $y > 0$ can be calculated by summing contributions from each of the line charges,

$$\phi - \phi_0 = -\frac{\lambda}{4\pi\varepsilon_1} \ln\left(\frac{(x+a)^2 + (y-b)^2}{(x-a)^2 + (y-b)^2}\right) - \frac{\lambda'}{4\pi\varepsilon_1} \ln\left(\frac{(x-a)^2 + (y+b)^2}{(x+a)^2 + (y+b)^2}\right), \tag{2}$$

Corresponding electric fields are given by $E = -\nabla\phi$.

First, expression that satisfies the boundary condition over the target surface was formulated. It was then tested to determine if it satisfied the other boundary conditions. Electrostatic boundary conditions at the target surface ($y = 0$) are given by,

$$\varepsilon_1 E_{1,\mathrm{n}} = \varepsilon_2 E_{2,\mathrm{n}} \text{ and} \tag{3}$$

$$E_{1,\mathrm{t}} = E_{2,\mathrm{t}}, \tag{4}$$

where $E_{i,n}$ and $E_{i,t}$ denote normal component and tangential component of electric field, respectively. Substituting Eq. (2) into Eqs. (3) and (4) yields

$$\lambda ' = \frac{\varepsilon_2 - \varepsilon_1}{\varepsilon_2 + \varepsilon_1} \lambda. \tag{5}$$

Equipotential lines drawn from Eq. (2) with Eq. (5) are circles when $\varepsilon_1 = \varepsilon_2$ as shown in Fig. 2D. To approximate the values of parameters λ, a, and b, ε_1 is assumed to be equal to ε_2 and then the parameter values are determined as functions of ϕ_o, R_o, and R_i, which are given by

$$\lambda = \frac{2\pi\varepsilon_1\phi_o}{\cosh^{-1}(R_o / R_i)}, \ a = \sqrt{R_o^2 - R_i^2}, \ \text{and} \ b = R_o, \tag{6}$$

where R_i and R_o are inner and outer diameters of the silicone tube, respectively.

Therefore, the electric potential at $y > 0$ is given by

$$\phi - \phi_0 = -\frac{\phi_0}{2\cosh^{-1}(R_o / R_i)} \ln \left[\frac{(x + \sqrt{R_o^2 - R_i^2})^2 + (y - R_o)^2}{(x - \sqrt{R_o^2 - R_i^2})^2 + (y - R_o)^2} \left(\frac{(x - \sqrt{R_o^2 - R_i^2})^2 + (y + R_o)^2}{(x + \sqrt{R_o^2 - R_i^2})^2 + (y + R_o)^2} \right)^{\frac{\varepsilon_2 - \varepsilon_1}{\varepsilon_2 + \varepsilon_1}} \right]. \tag{7}$$

The induced charge due to the external field can be written as

$$\sigma = \mathbf{n} \cdot \varepsilon_0 \mathbf{E}_1 \left(1 - \frac{\varepsilon_1}{\varepsilon_2} \right) \tag{8}$$

The attractive force exerted on the target surface, $F = -\int_{-\infty}^{\infty} \sigma \frac{\partial \phi}{\partial y} dx$, is calculated as

$$F = \pi\Phi_0{}^2 \frac{(R_o{}^2 - R_i{}^2)}{R_o(2R_o{}^2 - R_i{}^2)\left\{\cosh^{-1}\left(\frac{R_o}{R_i}\right)\right\}^2} \varepsilon_0 \left(1 - \frac{\varepsilon_1}{\varepsilon_2} \right) \left(\frac{2\varepsilon_2}{\varepsilon_1 + \varepsilon_2} \right)^2 \tag{9}$$

Electrochemical reaction of ISW.

No electrochemical reaction occurs in the ISW even if high voltage is applied. Equivalent circuit of the ISW is described in fig. S7. At equilibrium, the voltage applied between the two threads is carried entirely by the two electrical double layers and the dielectric, $V_{applied} = 2V_{EDL} + V_D$, where V_{EDL} is the voltage across electrical double layer and V_D is the voltage across dielectrics. In the response to the applied voltage, the three capacitors add the same amount of charge, $c_D A_D V_D = c_{EDL} A_{EDL} V_{EDL}$, where A_{EDL} is area of the electrical double layer, A_D is area of the dielectric, c_{EDL} is areal capacitance of the electrical double layer, and c_D is areal capacitance of the dielectrics. In this study, the ratio between voltage was on the order of $V_{EDL}/V_D \sim 10^{-5}$, because the ratio between area was on the order of $A_{EDL}/A_D \sim 0.01$ and ratio between areal capacitance was on the order of $c_{EDL}/c_D \sim 10^7$. Thus, voltage across the electrical double layer V_{EDL} was well below 1 V when the applied voltage is on the order of $V_{applied} \sim 10\ kV$ and no electrochemical reaction occurred except for the electrochemical reaction caused by minute leakage current, which was less than 2.3 nA/cm (fig. S8) (3).

Dielectric breakdown of ISW

Although electrochemical reaction is negligible, ISW can undergo dielectric breakdown if the electric field across dielectrics exceeds the dielectric strength of silicone rubber (50 ~ 100 kV/mm) (9). Moreover, all components of the ISW are made of soft materials and can therefore be stretched. A decrease in thickness of dielectric caused by stretching leads gels in a pair of ISW to be closer to each other, and thus generates a stronger electric field. It can cause dielectric breakdown of the stretched ISW under lower applied voltage than the breakdown voltage of unstretched ISW. Thus, considering unpredictable deformation, ISWs were utilized at 5 kV of DC voltage, which are far less than the average breakdown voltage of the unstretched ISW (fig. S9). According to Fig. 2, I and J and movie S3, ISW operated stably when 50% of strain was applied.

Viscoelasticity of silicone rubber can cause a time-dependent deformation of ISW, making the silicone rubber thinner while the high voltage is applied (44). Thus, the electric field across the silicone rubber becomes stronger over time under same applied voltage. It can raise the durability concerns for long time operation of ISW. Therefore, it is essential to turn on the electrostatic adhesion only when target is nearby, and sensing capability of ISW can reduce the concerns about time-dependent breakdown.

Despite the efforts to avoid failure, unexpected breakdown can still occur. When breakdown occurs, sudden increase of the leakage current causes the destruction of ISW. It can raise safety concerns for high voltage application of ISW. Therefore, current is always measured, so that the applied voltage could be shut down when sudden increase of leakage current is detected (fig. S10).

Effect of static objects to sensing capability of ISW

Figure. S12 is a schematic description of the sensing mechanism and the effect of static objects around the ISW. Approach of a charged target to an ISW forms electrical double layer between interface of platinum electrode and gel, which induced potential difference across external load. Sensing capability of ISW is realized by measuring the voltages across the external load ($t = t_2$). Then, electrons from the ground gradually flow through the external load to neutralize the potential difference ($t = t_3$). Induced voltage across external load converges to zero, when the quantity of electric charge of supplied electrons equals that of ions built up in the electrical double layer ($t = t_4$). Thus, even if charged objects exists around the ISW, they do not affect the sensing capability of ISW unless they move.

When the same voltage was induced across external load, current decreased as the resistance of external load increased. Thus, recovery time of electrostatic sensing depends on the resistance of external load (fig. S13). As the resistance of external load increased from 1 to 20 gigohm, recovery time was increased from 2.5 to 37.9 s. Even though ISW equipped with external load of 5 gigohm to acquire high sensitivity as shown in Fig. 3H, adopting external load of lower resistance can lead to reduced recovery time.

Effect of ambient electrical noise to sensing capability of ISW

To demonstrate sensing capability of ISW under practical conditions, an experiment was conducted outside of Faraday cage (fig. S16). Electrical noise was increased up to ~ 130 mV$_{pp}$ when induced voltage was measured without Faraday cage, which was 10 times higher than the case of measuring the induced voltage with Faraday cage (Fig. 3K). Although electrical noise increased, the ISW successfully sensed the approach of a target and then interacted with programmed computers.

Effects of surface treatments on electrostatic vibration cleaning.

A liquid droplet hanging on a substrate can be detached when an external body force exceeds the adhesion force due to surface tension, which can be written as

$$F_{\text{ext}} > \pi L \gamma \sin \theta, \tag{10}$$

where L is the length of the contact line, γ is the surface tension, and θ is the contact angle. When the vibration frequency matches the resonant frequency of the ISW, the vibration amplitude is maximized. Thus, when resonance frequency is included in the range of frequency sweep, most droplets will bounce off by their inertia (45). However, if the detachment condition, Eq. (10), is not satisfied, not all pendant droplets are detached during the frequency sweep. The adhesion force is mitigated by increasing the contact angle, then decreasing the length of contact line via surface treatment over the silicone rubber. The surface treatment results into a droplet cleaning under the same condition, as shown in Fig. 4J.

Capturing

Essential function of the web but causing contaminations by adhesion	
Spiderweb	**ISW**
Viscous adhesion to capture preys	**Electrostatic adhesion** to capture targets
Stretchability to enhance adaptability	**Stretchability** to enhance adaptability
Translucency for passive camouflage	**Translucency** for passive camouflage
Reinforcing the structure by structural thread	**Reinforcing the structure** by nylon thread

Sensing

Minimizing contamination by reducing the adhesion	
Spiderweb	**ISW**
Minimizing contamination by building minimal webs	**Minimizing contamination** by turning off the adhesion
Sensing vibration caused by contact of preys	**Sensing voltage** caused by approach of targets
Reinforcing the adhesion by wrapping additional webs	**Reinforcing the adhesion** by turning on the adhesion

Cleaning

Eliminating contaminants to recover the adhesion	
Spiderweb	**ISW**
Using mechanical stress to deform webs	**Using Maxwell stress** to deform webs
Eliminating contaminants by releasing webs	**Eliminating contaminants** by releasing webs

Fig. S1. ISWs emulating the optimized capturing strategies of spiders.

Spiders have used their own unique capturing strategies. ISWs are made to emulate spider's outstanding capturing strategies.
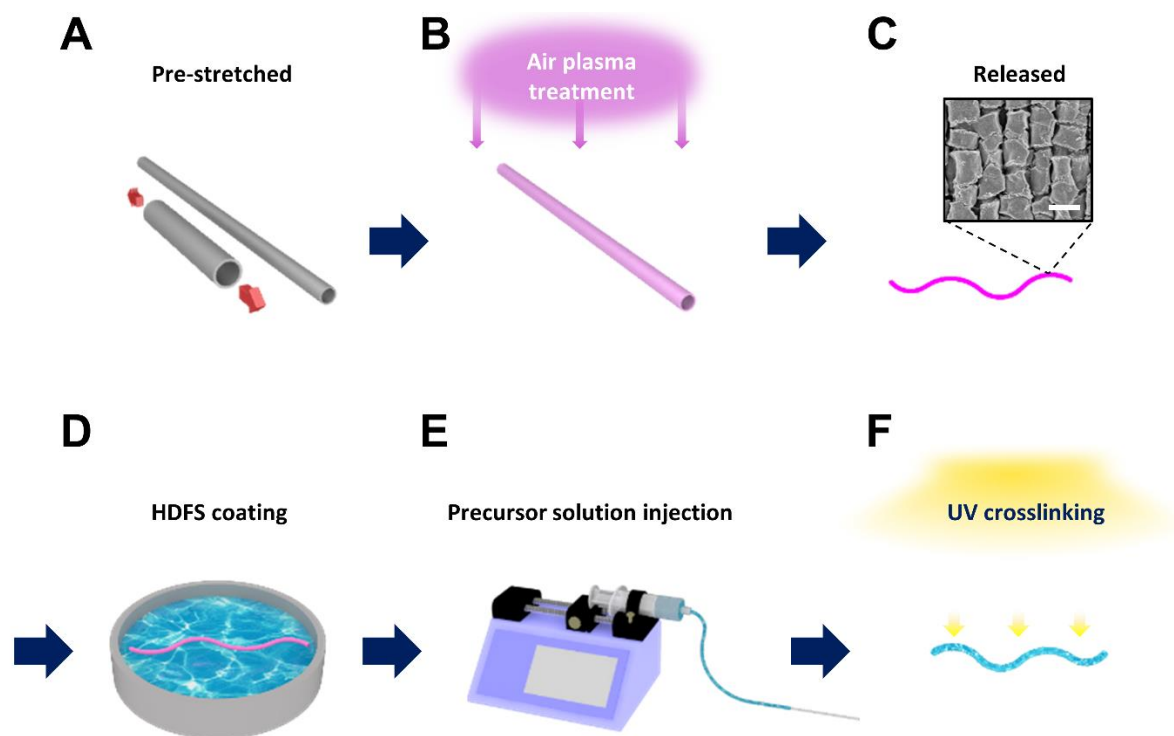
Fig. S2. Fabrication process of an ISW.

(**A** to **F**) Pre-stretched silicone tubes (A) were treated with air plasma (B) and released to obtain wrinkled surfaces (C). Treated tubes were immersed in a solution with HDFS for self-assembly monolayer coating (D) (*25*). Organogel precursor solution was injected into the tube (E) followed by 365 nm UV irradiation in inert condition for 5 minutes (F). Scale bar, 1 μm.
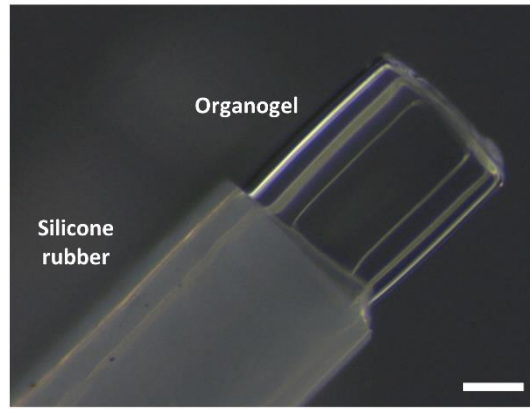
Fig. S3. Magnified image of an ISW.

Transparent organogel is capsulated with translucent silicone rubber. Scale bar, 200 μm.
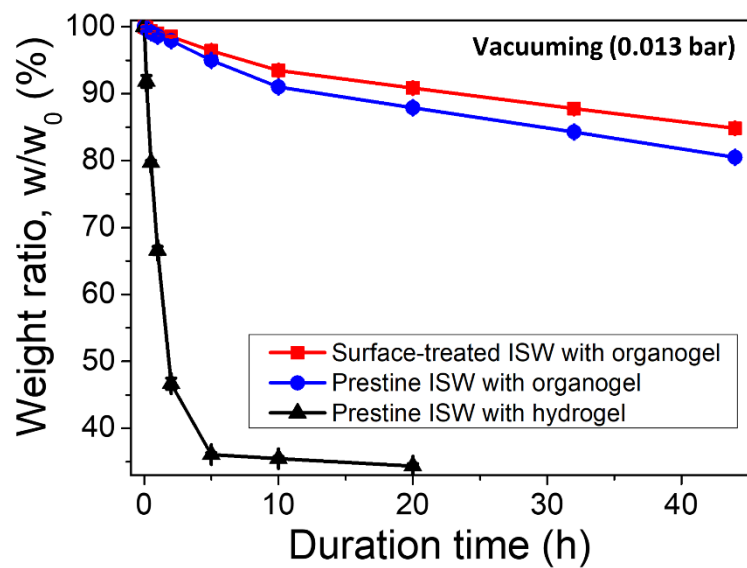
Fig. S4. Anti-dehydration capability of ISWs under harsh conditions.

Organogel with a vapor pressure of 0.5 kPa evaporates relatively slower than hydrogel with a vapor pressure of 2.3 kPa (*7*). Surface treatment prevented evaporation of organogel by lowering the vapor permittivity of silicone rubber (*25*). Error bars represent SD (n=3).

**Structural
thread**
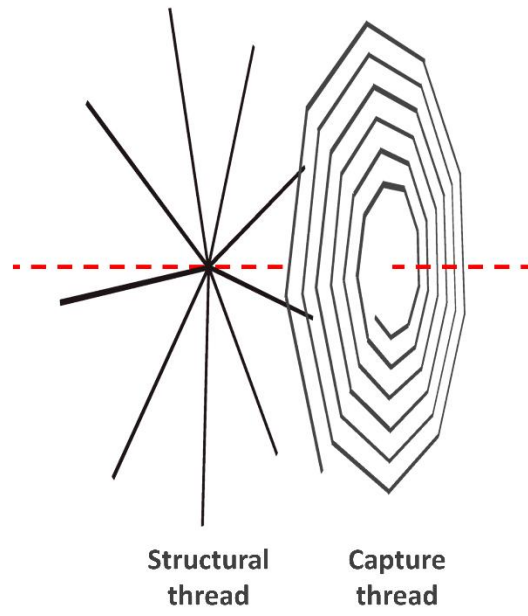
**Capture
thread**

Fig. S5. Exploded view of orb spiderwebs.

Spiders spin adhesive, stretchable, and translucent capture thread on strong structural thread.

A

B
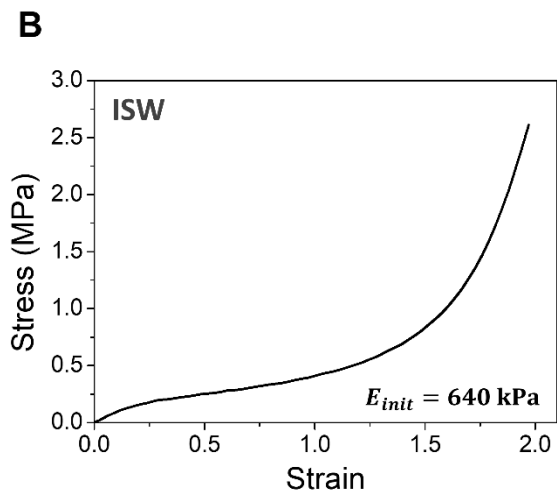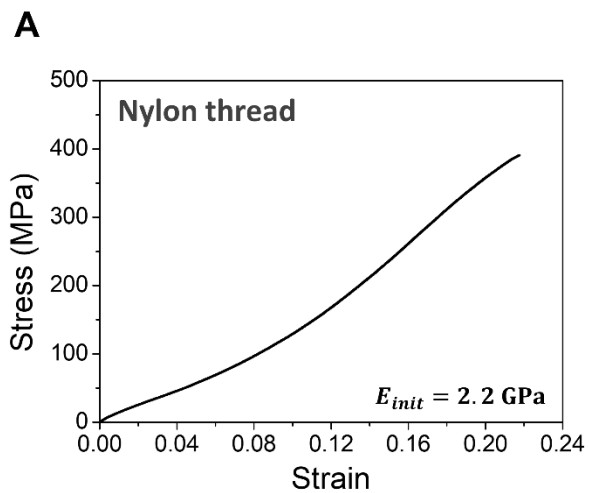
Fig. S6. Stress-strain curve of tensile test.

(A) Stiffness and extensibilities of nylon thread were 2.2 GPa and 0.21, respectively. **(B)** Stiffness and extensibilities of ISW were 640 kPa and 1.9, respectively.
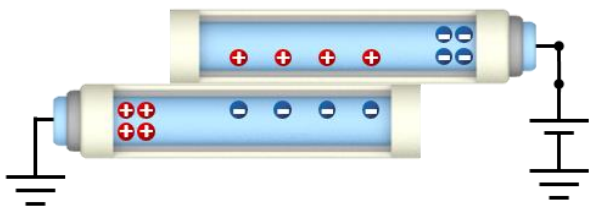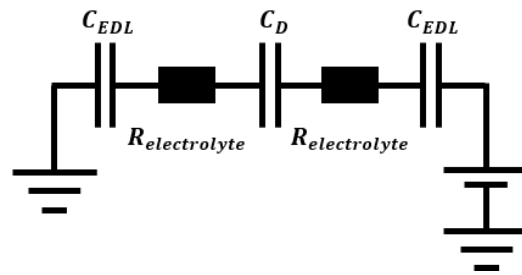
Fig. S7. Equivalent circuit of electrostatic adhesion capturing.

(**A** and **B**) Schematics of electrostatic adhesion capturing (A) and its equivalent circuit (B).
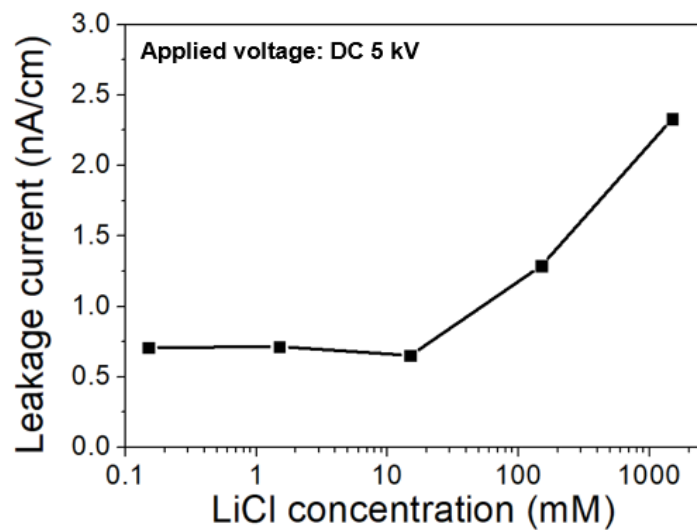
Fig. S8. Leakage current of ISW.

In a wide range of LiCl concentrations from 0.15 mM to 1.5 M, there was insignificant leakage current.
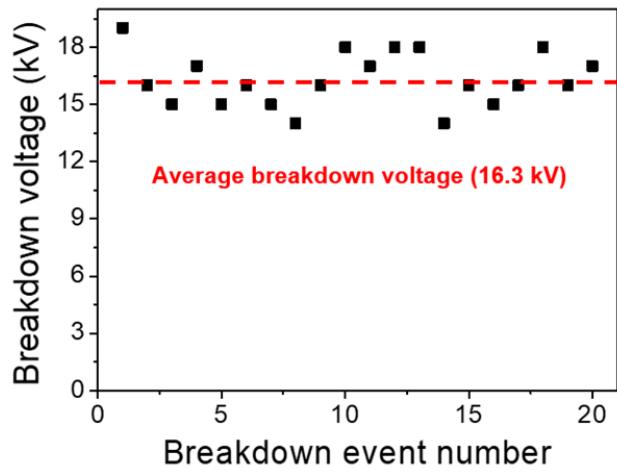
Fig. S9. Breakdown voltages of ISW.

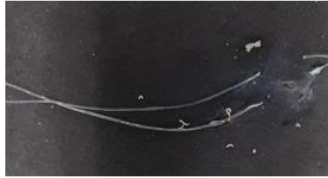Maximum applied voltages that ISW can endure were measured. The average breakdown voltage was measured as 16.3 kV.
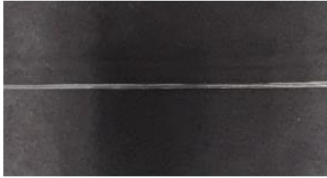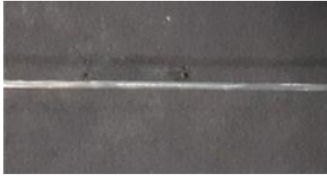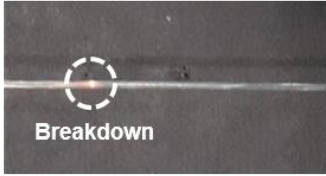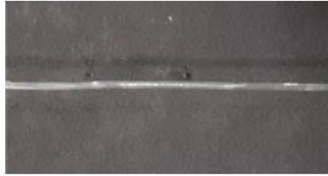
Sample type	Applied voltage (DC 18 kV)		
	Before	Breakdown	After
w/o current limitation			
w/ current limitation		Breakdown	

Fig. S10. Dielectric breakdown behavior of ISW.

When breakdown occurs, sudden increase of the leakage current causes the destruction of ISW. Therefore, leakage current was measured, so that the applied voltage could be shut down when increase of leakage current is detected.
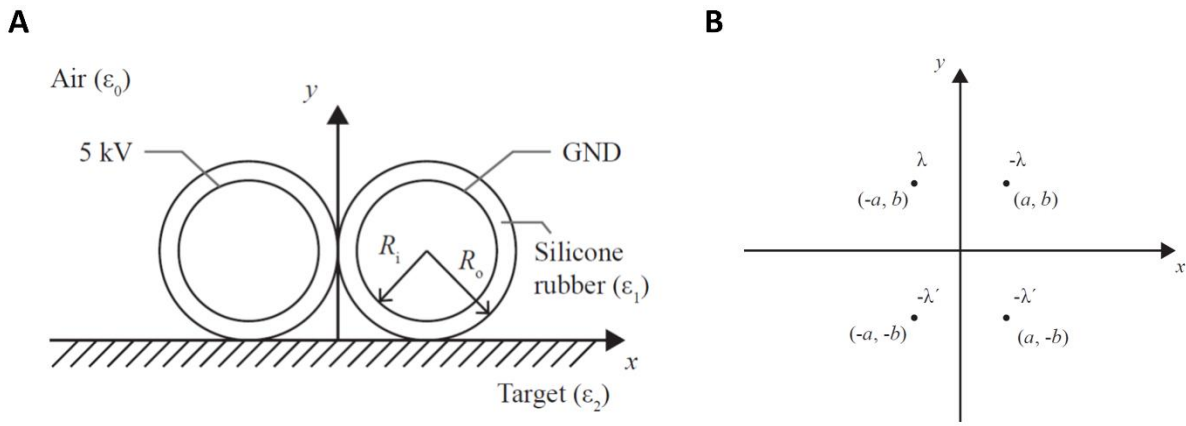
Fig. S11. Problem definition for deriving mathematical expression of electrostatic adhesion force.

(**A**) Cross-sectional schematic of an ISW and a target while they are attached. (**B**) Schematic of the image charge method to solve the given problem. Each imaginary wire running out of the xy plane carries a uniform line charge, as denoted near the position.
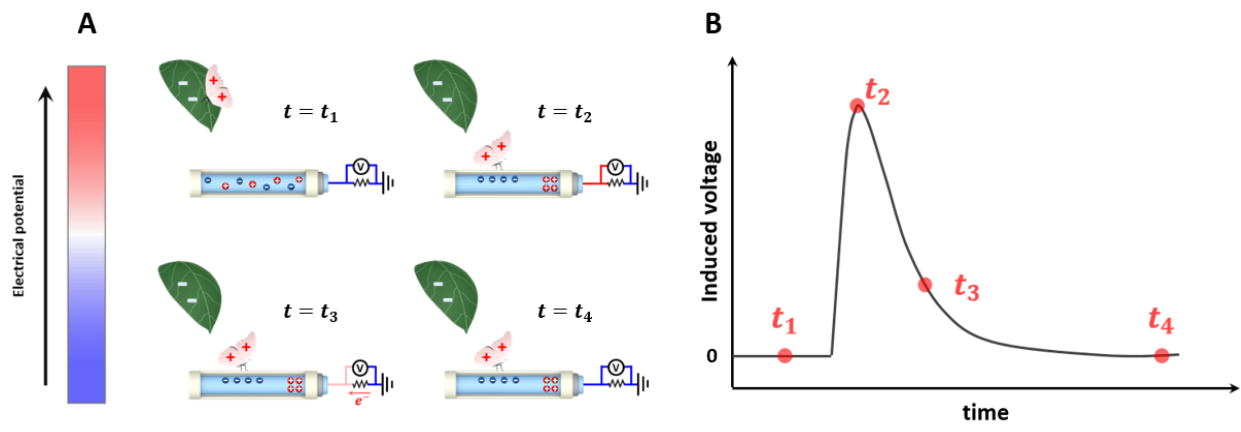
Fig. S12. Schematic describing the effect of static objects around the ISW.

(**A** and **B**) Schematic describing a detailed sensing mechanism (**A**) and graph of induced voltage over time (**B**). Even if charged objects exist around the ISW, they do not affect the sensing capability of ISW unless they move.
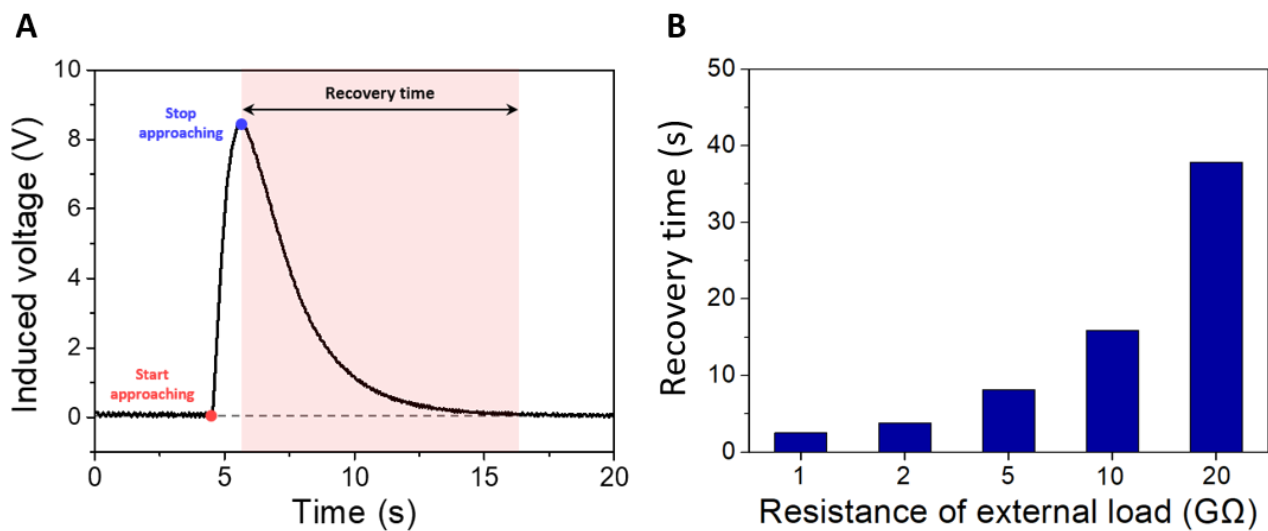
Fig. S13. Experimental results describing the effect of static objects around the ISW. (**A**) Recovery time is the time required for the induced voltage to converge to zero after the approaching object stopped. (**B**) As the resistance of external load increased from 1 to 20 gigohm, recovery time increased from 2.5 to 37.9 s.
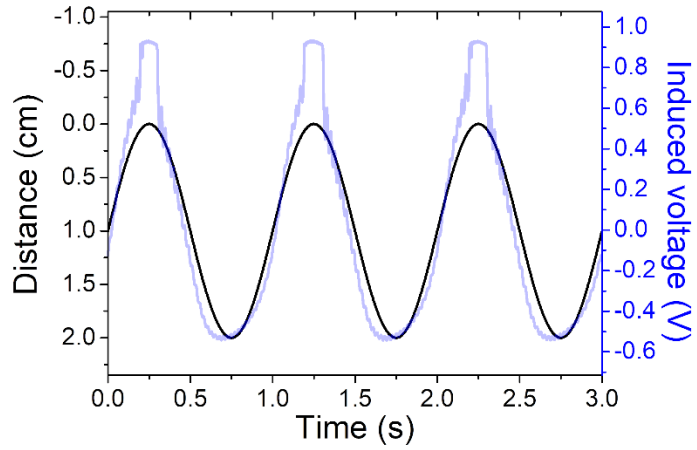
Fig. S14. Induced voltage when a target contacts ISW.

The sensing capability was tested under sinusoidal wave of 1 Hz. It is possible to sense the contact of targets by measuring the induced voltage.
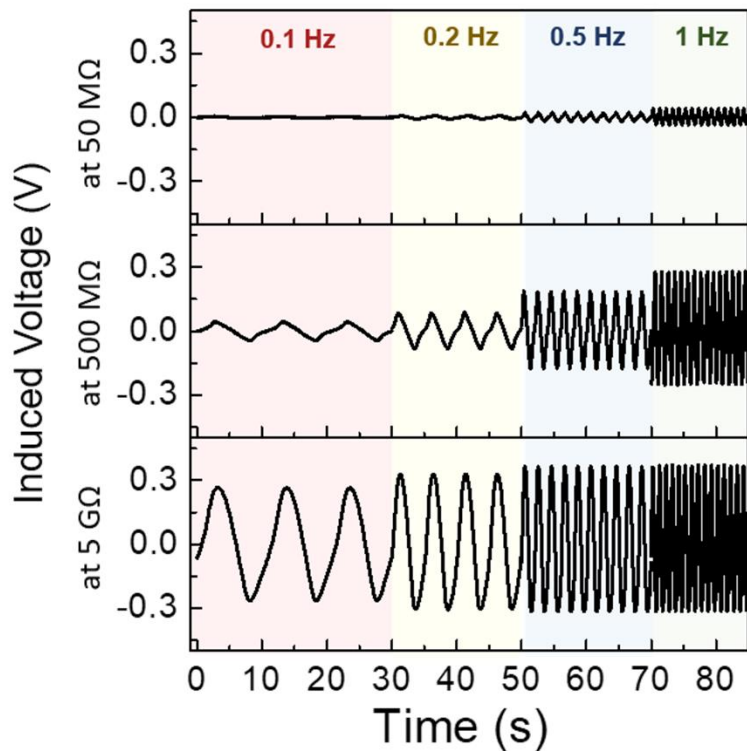
Fig. S15. Induced voltages measured with various resistances of external loads and approaching speeds of a target.

High resistance of external load increased the effect of RC delay. When delay is increased, the ISW exhibits higher sensitivity.

A

Charging materials: PFA
External load: 5 GΩ

ON-state

OFF-state

$\triangle$d: 1.5 cm
Target: Glass
Reference distance (d_0): 1 cm

Induced voltage (V) — Time (s)

B

Sample state
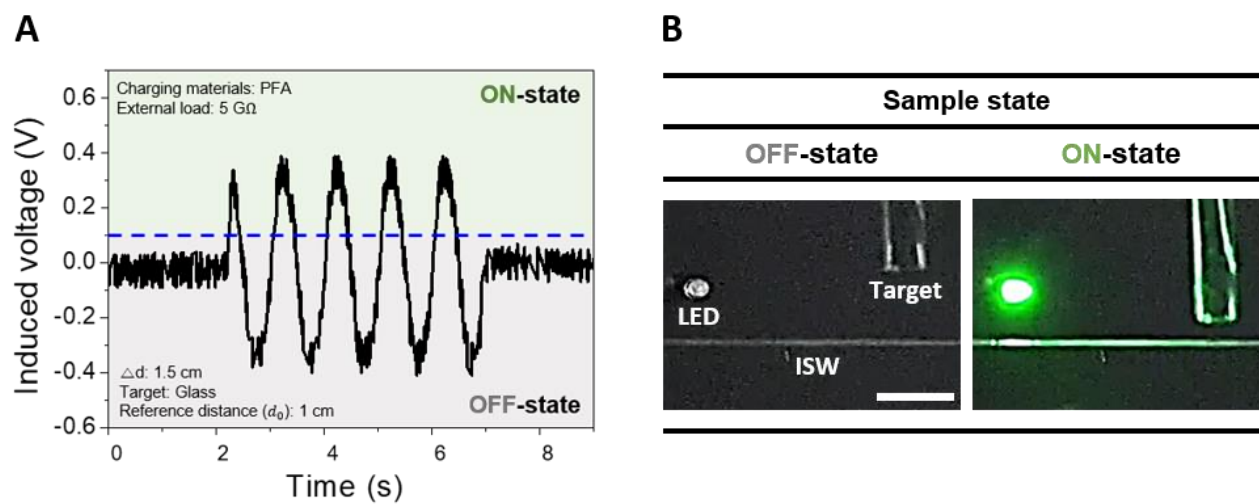
OFF-state | ON-state

LED
Target
ISW

Fig. S16. Demonstration of electrostatic induction sensing under practical conditions.
(**A** and **B**) A green light emitting diode (LED) was turned on when the induced voltage exceeds a threshold voltage of
0.1 V. Scale bar, 1 cm.

Table S1. Tensile mechanical properties of spiderwebs and ISWs.

Structural threads are 3,300 times stiffer than capture threads, while their extensibility is 10 times lower (*11*). Similar to spiderwebs, nylon threads are 3,400 times stiffer than ISW, while their extensibility is 9 times lower

Materials	Role	Stiffness, E_{init} (MPa)	Ratio	Extensibility, ε_{max}	Ratio
Capture thread	Adhesion	3.0		2.7	
			3300		0.10
Structural thread	Framework	10000		0.27	
Ionic spiderweb	Adhesion	0.64		1.9	
			3400		0.11
Nylon thread	Framework	2200		0.21	

Movie S1. Slingshot cleaning of spiders.

Spiders pull and rapidly release their webs in a manner similar to a slingshot, causing the contaminants on webs to bounce off by inertia force, thus recovering the capturing capability of the webs (Fig. 1B).

Movie S2. Measurement of electrostatic adhesion force.

For all measurements of electrostatic adhesion force, a universal-testing-machine with a static load cell was used at a fixed receding rate of 3 mm/min. Targets and ISWs were fixed in place with a custom acrylic holder.

Movie S3. Stretchable electrostatic adhesion net.

To demonstrate capturing capability, four pairs of ISWs were fixed at 1 cm intervals in a zigzag pattern and tilted approximately 80° relative to the horizontal (Fig. 2J). Because of the simple structure, 0.2 g of ISWs was able to capture 6.8 g of an aluminum plate. The ISWs readily expanded to 50% of strain in the longitudinal direction and were able to capture a heavier target (13.6 g). Because the stretched ISWs were under tension, they showed less deflection when capturing a target.

Movie S4. Test of contamination.

Contamination was tested using a cubic-shaped acrylic system (1.73 L). ISWs were set at the center of the system. Each ISW was kept under adhesion ON-state and OFF-state, respectively. Ten grams of silica powder with an average particle diameter of 50 μm was then scattered using a fan for 50 s, and adhesion force was measured every 10 s during this time.

Movie S5. Sensing by electrostatic induction.

When the induced voltage exceeded a threshold voltage of 0.1 V for sensing, the computer allowed the power source to operate. As shown in Fig. 3 (K and L), a green light emitting diode (LED) was turned on when an ISW sensed the approach of a target.

Movie S6. Measurement of vibration amplitude.

To measure the vibration amplitude of ISWs, a high-speed camera that could run up to 6,242 frames per second was used.

Movie S7. Cleaning by electrostatic vibration.

Cleaning capabilities of pristine and surface-treated ISWs were investigated using a frequency sweep of the applied v oltage (Fig. 4J). Droplets of water were initially suspended from each ISW. A droplet on a surface-treated ISW was cl eaned during the vibration, whereas a droplet on a pristine ISW was not cleaned off.

Movie S8. Ionic spiderwebs.

An ISW was fabricated in the form of an orb-web, as shown in Fig. 5A. A pair of threads was fixed on nylon threads as a framework (Fig. 5B). The distance between the pairs was 1 cm (d_o) and the distance between threads in a pair

was 3 mm (d_i). The ISW exhibits passive camouflage in diverse environments (such as a forest, fallen leaves, a brick wall, and the floor of a building) because it is transparent and thin, as shown in Fig. 5C. In an attempt to enhance the adhesion force, the ISW was tilted to 80° from the horizontal. In the initial state, the ISW was contaminated with dust such as polyurethane particles (Fig. 5D, i). During cleaning, a frequency of the applied voltage was swept from 30 to 60 Hz for 200 s, and the dust that covered the ISW was notably cleaned (Fig. 5D, ii). After the cleaning, the ISW was turned to sensing mode with no applied voltage. When an approaching target caused the induced voltage to exceed the threshold voltage of 1 V, the ISW was rapidly converted to capturing mode (Fig. 5D, iii). Various types of materials—such as a leaf (0.4 g), PMMA (3.1 g), glass (8.5 g), and aluminum (11 g)—were tightly captured by the electrostatic adhesion of the ISW (Fig. 5D, iv). After performing the mission, the targets were released by application of 30 Hz of AC voltage to the ISW (Fig. 5D, v).